

GREEN GALAXIES IN THE COSMOS FIELD

Zhizheng Pan^{1,2}, Xu Kong^{1,2} and Lulu Fan^{1,2}

panzz@mail.ustc.edu.cn, xkong@ustc.edu.cn

ABSTRACT

We present a research of morphologies, spectra and environments of ≈ 2350 “green valley” galaxies at $0.2 < z < 1.0$ in the COSMOS field. The bimodality of dust-corrected $\text{NUV}-r^+$ color is used to define “green valley” (thereafter, GV), which removes dusty star-forming galaxies from truly transiting galaxies between blue cloud and red sequence. Morphological parameters of green galaxies are intermediate between those of blue and red galaxy populations, both on the Gini–Asymmetry and the Gini– M_{20} planes. Approximately 60% to 70% green disk galaxies have intermediate or big bulges, and only 5% to 10% are pure disk systems, based on the morphological classification with Zurich Estimator of Structural Types (ZEST). The obtained average spectra of green galaxies are intermediate between blue and red ones in terms of [O II], $\text{H}\alpha$ and $\text{H}\beta$ emission lines. Stellar population synthesis on the average spectra show that green galaxies are averagely older than blue galaxies, but younger than red galaxies. Green galaxies have similar projected galaxy density (Σ_{10}) distribution with blue galaxies at $z > 0.7$. At $z < 0.7$, the fractions of $M_* < 10^{10.0} M_\odot$ green galaxies located in dense environment are found to be significantly larger than those of blue galaxies. The morphological and spectral properties of green galaxies are consistent with the transiting population between blue cloud and red sequence. The possible mechanisms for quenching star formation activities in green galaxies are discussed. The importance of AGN feedback cannot be well constrained in our study. Finally, our findings suggest that environment conditions, most likely starvation and harassment, significantly affect the transformation of $M_* < 10^{10.0} M_\odot$ blue galaxies into red galaxies, especially at $z < 0.5$.

Subject headings: galaxies: evolution — galaxies: formation — galaxies: stellar content — galaxies: interactions

¹Center of Astrophysics, University of Science and Technology of China, Hefei 230026, China

²Key Laboratory for Research in Galaxies and Cosmology, Chinese Academy of Sciences, Hefei 230026, China

1. Introduction

Many observational properties of galaxies in local universe, such as optical colors (Strateva et al. 2001; Baldry et al. 2004), spectral indices (Kauffmann et al. 2003), morphological parameters (Driver et al. 2006), exhibit bimodal distributions. Deeper surveys such as DEEP2 (Willmer et al. 2006), COSMOS (Zamojski et al. 2007) and NEWFIRM (Brammer et al. 2009) have revealed that the bimodality of galaxy properties exists up to $z \approx 2$. Generally, galaxies are categorized into two main populations: red quiescent galaxies and blue star-forming galaxies. The red quiescent galaxies, mainly early-type galaxies (ETGs), lie on a relative narrow ridge (the red sequence) in the color-magnitude diagram (CMD). The blue star-forming galaxies, mainly late-type galaxies (LTGs), are distributed throughout the so-called “blue cloud”. Galaxies located in the region between blue cloud and red sequence are called “green valley” galaxies (thereafter, green galaxies).

Studies on galaxy evolution reported that red galaxies have grown in stellar mass by a factor of 2 to 4, whereas the number density of luminous blue galaxies has dropped strongly since $z \approx 1$ (Bell et al. 2004; Faber et al. 2007; Bolzonella et al. 2010; Ilbert et al. 2010; Brammer et al. 2011). The transformation of a significant fraction of blue galaxies into red galaxies during this cosmic time has been suggested by some previous works (Faber et al. 2007; Pozzetti et al. 2010). However, the transiting timescale must be short (Faber et al. 2007; Martin et al. 2007; Balogh et al. 2011), since the bimodality will never be observed if the transiting timescale is over a Hubble time. Green galaxies are therefore be considered as a transiting population migrating towards the red sequence. However, only a few studies have focused on this less prominent population. Some works reported that a large fraction of green galaxies are not truly transiting, but are dusty, star-forming galaxies (Brammer et al. 2009; Salim et al. 2009).

The physical properties of green galaxies have been revealed, to some extent, in earlier works. Based on the DEEP2 redshift survey, Coil et al. (2008) found that the co-added spectra of green galaxies have higher $[\text{O III}]/\text{H}\beta$ ratio than the spectra of blue galaxies at $z \approx 1$. Furthermore, the large-scale clustering amplitude of green galaxies is similar to that of red galaxies. However, green galaxies show similar clustering amplitude with blue galaxies at a scale of < 1 Mpc. Using SDSS main galaxy sample, Zehavi et al. (2011) showed that green galaxies have a clustering amplitude that can be found between amplitudes of red and blue galaxies. Balogh et al. (2011) reported that they discovered a large transiting galaxy population in X-ray groups at $0.85 < z < 1.0$ in the COSMOS field, and these galaxies reside in the optical GV. Most of these galaxies have bulges and small disk components, with half of them showing prominent $\text{H}\delta$ absorption lines. Mendez et al. (2011) studied the morphologies of green galaxies in the AEGIS field and found that green galaxies are intermediate between blue and red populations in terms of concentration, asymmetry and morphological type; furthermore, removing dusty galaxies from the green galaxy sample would not alter this result. Goncalves et al. (2012) studied the star formation history (SFH)

of about 100 GV galaxies at $z \approx 0.8$ based on Keck spectra, and found that the transformation happened more rapidly for more massive galaxies. Most previous studies are based on very small samples, or focused on a very narrow redshift range. A specific study on physical properties and redshift evolution of this population can be conducted using a large and homogeneous sample that spans a wide redshift range, along with deep multi-band photometry, spectra, high-resolution images, etc.

One of the emerged key questions is: which physical mechanisms are responsible for quenching star formation activities in blue galaxies, then resulting the transformation? Different star formation-quenching mechanisms have been proposed. Of these, merger can effectively convert LTGs into ETGs, both in observation and simulation. A major merger can change the overall galaxy morphology as well as form bulge and trigger starburst, which can quickly consume gas, or expel them through shocks from supernovae feedback (Springel et al. 2005; Robertson et al. 2006). Another possible quenching mechanism is the active galactic nucleus (AGN) feedback. In this scenario, the AGNs heat gas to prevent them forming new stars (Bower et al. 2006; Tremonti et al. 2007). The AGN feedback scenario is observationally supported by X-ray imaging of evacuated cavities around massive galaxies (McNamara et al. 2000, 2007). Interestingly, some studies found that the AGN detection rate is high in GV (Nandra et al. 2007; Coil et al. 2009). Meanwhile, environmental effects can lead to quenching, as suggested in a great deal of works. For example, studies based on *Hubble Space Telescope* (*HST*) showed that distant clusters have larger fractions of LTGs than local clusters (Dressler et al. 1997; Fasano et al. 2000; Lubin et al. 2002). These studies found the fraction of S0 galaxies has significantly increased since $z \sim 0.7$, whereas the fraction of spiral galaxies decreased significantly. The most favored explanation is that the dense environment can effectively quench star formation activities in blue galaxies and turn them into S0 galaxies (Vogt et al. 2004; Moran et al. 2007).

In this paper, we use the COSMOS data to study the transiting population and constrain mechanisms that lead to star formation quenching. The COSMOS survey (Scoville et al. 2007), the largest contiguous survey with *HST*, provides a combined data set including multi-band photometry covering X-ray, UV, optical, infrared, millimeter to radio (Bertoldi et al. 2007; Capak et al. 2007a; Hasinger et al. 2007; Sanders et al. 2007; Zamojski et al. 2007). The morphological parameters measured using the Advanced Camera for Surveys (ACS) imaging are also available (Koekemoer et al. 2007). The zCOSMOS survey (Lilly et al. 2007) provides approximately 10,000 galaxy spectra in 1.4 deg² COSMOS field, thereby facilitating the exploration of spectral characters. The photometric redshifts of COSMOS galaxies are extremely accurate (Ilbert et al. 2009), and allows the measurement of galaxy environment. Thus, the COSMOS provides an ideal data set for selecting a large transiting galaxy sample, and for studying this sample in detail.

This paper is organized as follows. Section 2 presents the data set used for the study. Section

3 defines the red, green and blue galaxies, as well as the mass limits. Section 4 presents the morphologies, stacked spectra and environments of red, green and blue galaxies. Section 5 discusses the possible mechanisms responsible for quenching star formation activities. A summary of conclusions is presented in Section 6. Throughout this paper, a concordance Λ CDM cosmology with $\Omega_m = 0.3$, $\Omega_\Lambda = 0.7$, $H_0 = 70 \text{ km s}^{-1}\text{Mpc}^{-1}$ is assumed. All magnitudes are quoted with the AB normalization, unless explicitly noted.

2. DATA

2.1. Photometric Redshift Catalog

The large samples required for this work necessitate the use of photometric redshifts. We use the COSMOS photometric redshift catalog (Version 1.8) published by Ilbert et al. (2009). Accurate photometric redshifts were computed by 30 broad, intermediate, and narrowband photometry, which included the UV (*Galaxy Evolution Explorer*), optical–NIR (Subaru, Canada France Hawaii Telescope (CFHT), United Kingdom Infrared Telescope (UKIRT) and National Optical Astronomy Observatory), and mid-IR (Spitzer/IRAC). Ilbert et al. (2009) computed the photometric redshifts of the COSMOS galaxies using *Le Phare*¹ codes with a χ^2 template-fitting method, which included a novel treatment of the emission lines. To generate the photometric catalog, all images had been PSF-matched and fluxes were measured with SExtractor over an aperture with a diameter of $3''$ at the position of Subaru i^+ band detection. Ilbert et al. (2009) included 9 templates generated by Polletta et al. (2007) to fit the UV-to-mid-IR data. To recover the SED of blue galaxies, 12 additional templates were generated using BC03 model (Bruzual & Charlot, 2003) with starburst ages ranging from 0.03 to 3 Gyr. A comparison of the photometric and spectroscopic redshifts showed that the accuracy is $\sigma_{(z_{\text{phot}}-z_{\text{spec}})}/(1+z_{\text{spec}})=0.009$ for $i^+ < 22.5$, $\sigma_{(z_{\text{phot}}-z_{\text{spec}})}/(1+z_{\text{spec}})=0.011$ for $i^+ < 24.0$ and $\sigma_{(z_{\text{phot}}-z_{\text{spec}})}/(1+z_{\text{spec}})=0.057$ for $24.0 < i^+ < 25.0$ at $z < 1.25$. The SED template-fitting procedure also provided the best-fit rest-frame absolute magnitudes and dust-corrected NUV– r^+ color (thereafter (NUV– r^+)_{corr}). Other galaxy physical properties, such as stellar mass and instantaneous best-fit template star formation rate ($\text{SFR}_{\text{template}}$) were estimated adopting BC03 models, with a Chabrier IMF and an exponentially declining star formation history ($\text{SFR} \propto e^{-t/\tau}$, τ in the range 0.1 – 30 Gyr). To check the robustness of $\text{SFR}_{\text{template}}$, Ilbert et al. (2010) estimated the SFR_{IR} from IR luminosity L_{IR} , where L_{IR} was extrapolated from the Spitzer MIPS $24 \mu\text{m}$ flux using Dale & Helou (2002) library. $\text{SFR}_{\text{template}}$ and SFR_{IR} were found to be consistent upon comparison (see Figure 27 of Ilbert et al. 2010). In the following sections, SFR refers to the best-fit model SFR ($\text{SFR}_{\text{template}}$). More details please refer to Ilbert et al. (2010).

¹www.oamp.fr/people/arnouts/LE_PHARE.html

2.2. Morphological catalog

More than one million high-resolution galaxy images in COSMOS field are readily available for the morphological studies, as observed with *HST*. In previous works, automatic morphological classifications based on the parameters measured on the initial galaxy images were used to improve efficiency and avoid subjectivity (Capak et al. 2007b; Scarlata et al. 2007; Tasca et al. 2009). Here we briefly summarize the Zurich Estimator of Structure Types (ZEST) catalog (Scarlata et al. 2007) used in this paper.

ZEST classifies galaxy morphology based on a principal component analysis (PCA) of the galaxy structure nonparametric diagnostics, which include asymmetry A , concentration C , Gini coefficient G , the second-order moment of the brightest 20% galaxy pixels M_{20} , and the ellipticity of the light distribution ϵ . PCA shows that the first 3 PC variables contribute more than 90% of the original data set, thus can completely describe galaxy structure. ZEST classifies galaxy morphologies into three main types: elliptical galaxies ($T_{\text{ZEST}}=1$), disk galaxies ($T_{\text{ZEST}}=2$), and irregular galaxies ($T_{\text{ZEST}}=3$). Disk galaxies are assigned in 4 bins based on their “bulgeness” parameter (B_{ZEST}), which roughly correlates with the bulge-to-disk ratio $[B/D]$. For galaxies brighter than $i^+ = 22.5$, ZEST fits their surface brightness profile with Sérsic model. Higher values of B_{ZEST} indicate smaller bulges and larger disks, with $B_{\text{ZEST}}=[0,1,2,3]$, which correspond to the following range of Sérsic index n : $n \geq 2.5$, $1.25 \leq n \leq 2.5$, $0.75 \leq n \leq 1.25$ and $0 \leq n \leq 0.75$, respectively. The final ZEST catalog contains 131,532 sources down to $i^+ = 24.0$

The ZEST morphologies were tested using visual classification on $z = 0$ sample. It is found that the ZEST classifications agree well with the published morphologies. Among disk galaxies with $B_{\text{ZEST}}=0$, approximately 85% are classified as elliptical and S0–Sab type. Among disk galaxies with $B_{\text{ZEST}}=2$, the S0–Sab, Sb–Scd, and Sd types comprise 5%, 45% and 50%, respectively. The ZEST classifications begin to disintegrate at faint magnitude. Scarlata et al. (2007) quantified the efficiency of ZEST classifications by degrading the signal-to-noise ratio of bright galaxies with well determined morphologies. They reported that down to $i_{814\text{w}}=22.5$, the determination of the final T_{ZEST} or B_{ZEST} in 90% galaxies does not change. The fraction identified as the original morphological type is about 65% down to $i_{814\text{w}}=24.0$.

2.3. The 10k zCOSMOS Spectroscopic Sample

The zCOSMOS spectroscopic survey (Lilly et al. 2007) targets the galaxies in COSMOS field with the Visible Multi-Object Spectrograph (VIMOS) mounted on the ESO Very Large Telescope (VLT). The zCOSMOS survey has released about 10,000 galaxy spectra limited to $i^+ = 22.5$, covering a 1.4 deg^2 field of view. The spectra range from 5500\AA to 9700\AA , with a medium resolution of

$R \sim 600$. Redshifts were measured by the VIPGI software package. Results show that more than 97 % spectra at $0.5 < z < 1.25$ can yield very secure redshifts. Further information on zCOSMOS and the 10k sample are presented in Lilly et al. (2007).

3. Sample Selection

3.1. Green Galaxy Selection

Our parent sample contains 113,162 galaxies extracted from the COSMOS photometric redshift catalog (Version 1.8), with magnitudes and redshifts limited to $i^+ = 24.0$ and $z_{\text{phot}} = 1.2$, respectively. The magnitude and redshift limits ensure that our sample maintains high photometric redshift accuracy. There are many methods to define GV, usually exploiting the natural bimodal distribution of color indices such as $U - B$ (Nandra et al. 2007; Yan et al. 2011), $U - V$ (Brammer et al. 2009; Moresco et al. 2010) and $\text{NUV} - r$ (Wyder et al. 2007). In many dusty starburst galaxies, large amount of internal dust absorbs ultraviolet (UV) emission, resulting in red galaxy color. As mentioned in the first section, a significant fraction of green galaxies are virtually dust-obscured. To remove dusty star-forming galaxies from the real transiting galaxy sample, we use dust-corrected $\text{NUV} - r^+$ color to classify our sample.

Considering that considerable changes in extinction curves are expected from galaxy to galaxy, to get suitable dust extinction, Ilbert et al. (2009) used different extinction curves depending on the best-fit template obtained in the template-fitting procedure. Ilbert et al. (2009) applied a test on the zCOSMOS sample which with spectroscopic redshifts. They determined the best fit-template color excess $E(B - V)^{\text{best}}$ in the range of $E(B - V)^{\text{best}} = (0.0, 0.5)$, using only passbands with $\lambda > 3000(1+z)\text{\AA}$. As showed in Ilbert et al. (2009), the $E(B - V)^{\text{best}}$ value does not significantly depend on the adopted extinction law. Then, they compared the rest-frame observed magnitude m^{obs} and the predicted intrinsic magnitude without extinction $m_{\text{uncor}}^{\text{template}}$ at $\lambda_{\text{rest-frame}} < 3000\text{\AA}$, to discriminate between different extinction cures. Figure.4 in Ilbert et al. (2009) showed that for galaxies with template redder than starburst template SB3, the $m^{\text{obs}} - m_{\text{uncor}}^{\text{template}} / E(B - V)^{\text{best}}$ mainly follow the Prevot (1984) extinction curve. For galaxies bluer than SB3, the Calzetti et al. (2000) extinction law was found to be more appropriate. Ilbert et al. (2009) allowed an additional 2175\AA bump for the Calzetti law if a smaller χ^2 is produced. No reddening was allowed for galaxies redder than Sb .

Figure 1 shows $(\text{NUV} - r^+)_{\text{corr}}$ as a function of redshift for $M_* > 10^{8.0} M_{\odot}$ galaxies. The most remarkable feature is that $(\text{NUV} - r^+)_{\text{corr}}$ clearly shows bimodal distribution up to $z \approx 1$. In addition, the global galaxy color shows significant evolution since $z \approx 1$, for both red sequence galaxies and blue star-forming galaxies. Galaxies turn red towards low redshifts, which demonstrates that the global star formation activities decline with cosmic time (Bell et al. 2004; Brammer et al. 2011).

As the first step, we need to determine a criterion which can select homogeneous green galaxies without bias to red or blue galaxies at all redshifts. Ilbert et al. (2010) classified galaxies into “quiescent” with $(\text{NUV} - r^+)_{\text{corr}} > 3.5$, “high-activity” with $(\text{NUV} - r^+)_{\text{corr}} < 1.2$ and “intermediate activity” with $1.2 < (\text{NUV} - r^+)_{\text{corr}} < 3.5$. As global galaxy color evolves significantly with redshift, the sample selected with constant color cut over a wide redshift range can be biased toward red and blue galaxies at high and low redshifts, respectively. To minimize the bias, we have included the redshift evolution in our green galaxies selection scheme. In Figure 1, two green lines represent our selection criterion for green galaxy sample given by:

$$2.8 - 0.54z < (\text{NUV} - r^+)_{\text{corr}} < 3.4 - 0.54z, \quad (1)$$

where z is the photometric redshift. Red and blue galaxies are defined with $(\text{NUV} - r^+)_{\text{corr}} \geq 3.4 - 0.54z$ and $(\text{NUV} - r^+)_{\text{corr}} \leq 2.8 - 0.54z$, respectively. We use a non-zero slope in our selection criterion. The slope $\alpha = -0.54$ came from the linear fitting of median color for “quiescent” galaxies at 10 redshift bins within the range of $z = [0.2, 1.2]$. Our definition of green galaxies is much stricter than the “intermediate activity” in Ilbert et al. (2010) and considers the redshift evolution of galaxy color, which can help us to compare the truly transiting population with active and quiescent populations at the same cosmic epoch. The $(\text{NUV} - r^+)_{\text{corr}}$ color has been found to be well correlated with the specific star formation rate (sSFR) (defined as $\text{sSFR} = \text{SFR}/M_*$) (Salim et al. 2005). The median sSFR of our green galaxy sample is about $\log(\text{sSFR}) = -10.2$ at $z = 1.0$ and $\log(\text{sSFR}) = -10.8$ at $z = 0.2$. We find that more than 95 % galaxies in our sample lie on a very narrow ridge in $(\text{NUV} - r^+)_{\text{corr}}$ vs. sSFR diagram. About 3% of the galaxies have high sSFR and red $(\text{NUV} - r^+)_{\text{corr}}$, indicating that these may be extremely dusty starburst galaxies with underestimated dust extinction. We reject these galaxies from further analysis. Likewise, the $z < 0.2$ or $z > 1.0$ green galaxies were excluded because of the small sample size within these two redshift ranges.

It is worth noting that at $z \sim 0.1$, the GV is centered at $(\text{NUV} - r^+)_{\text{corr}} \sim 3.0$, which seems to be much bluer than when it was firstly reported in several GALEX papers (Wyder et al. 2007; Martin et al. 2007). Wyder et al. (2007) studied the UV-optical CMD using the GALEX and SDSS data, and found that GV is centered at $(\text{NUV} - r^+)_{\text{corr}} \sim 4$ (see Fig. 23 in Wyder et al 2007). The diversity is due to the different data depth used in these two papers. The data in Wyder et al. (2007) are limited to $r = 17.6$, which is much shallower than that used in this paper ($R_{\text{limit}} \simeq 25.0$). Our sample is volume-completed for the faintest source detected in Wyder et al. 2007 (about $M_r = -16.0$) out to $z \sim 0.25$. Thus, the volume-corrected CMD in Wyder et al. (2007) should be considered when comparing these two works. Keeping this in mind, excellent consistency between Figure 1 in this study and the Figure 25 in Wyder et al. (2007) is observed, which shows that the GV regions lie around $(\text{NUV} - r^+)_{\text{corr}} \sim 3$.

In a magnitude-limited sample, the minimum stellar mass for which observations were completed depends on the redshift and stellar mass-to-light ratio (M/L). Here, the low stellar mass

limits were defined to reduce the fraction of optical faint sources. To estimate the completeness mass we consider the galaxies in the faintest 20% of our sample and derive the stellar mass (M_{lim}) they would have if their apparent magnitude were equal to the limiting magnitude (i.e. $i^+ = 24.0$). Then we define as completeness mass the value of the 95% of the distribution of (M_{lim}): galaxies above this stellar mass limit define an 80% complete sample in stellar mass (see Pozzetti et al. 2010). We calculate the low mass limit for each redshift bin within the redshift range of $z = [0.2, 1.0]$, with bin size of $\Delta z = 0.1$. The values of low mass limits for the COSMOS sample used in the study are similar with those in literature (Tasca et al. 2009; Pozzetti et al. 2010; Giodini et al. 2012).

Figure 2 shows the color-mass relation for galaxies within $z = [0.2, 1.0]$. To separate the “red sequence” and “blue cloud” more clearly, we plot the contours of galaxy number density. The vertical lines show the low mass limits, which remove a larger fraction of active galaxies from the initial sample compared with red and green galaxies. In the literature on stellar mass functions, authors normally utilized different low mass limits for star-forming and quiescent populations (Pozzetti et al. 2010; Ilbert et al. 2010; Giodini et al. 2012). The current paper focused on GV galaxies located in a relatively narrow region in the CMD. For the green populations, their low mass limits do not significantly depend on color. For blue galaxies, the low mass limits maintain 47.6% and 12.8% of the initial sample at $z = [0.2, 0.3]$ and $z = [0.9, 1.0]$, respectively. For green galaxies, the mass limits maintain approximately 70% to 85% of the initial sample in all redshift bins. The conclusion of the present work is derived from the majority of green galaxies and are not significantly affected by the low mass limits.

Figure. 2 shows that there is a remarkable deficit of $M_* < 10^{10.0} M_{\odot}$ red galaxies at $z > 0.6$, which leads to difficulties in defining the GV utilizing color-magnitude (or color-mass) relation, as shown in some low-redshift studies. Green galaxies are mainly distributed at the minimum density regions in the diagram, or distribute at the reddest end of “blue cloud”, but these galaxies are till significantly redder than the bulks of “active” galaxies.

Figure 3 shows the color–color diagram ($M(\text{NUV}) - M(r^+)$ versus $M(r^+) - M(J)$). Optical–near-IR color is prevalently used to separate truly passive population from dusty star-forming galaxies (Williams et al. 2009; Bundy et al. 2010). In Figure 3, red galaxies are located in a tight clump in each redshift bin, which separate clearly from blue star-forming galaxies. Green galaxies mainly reside in the joint regions between red and blue galaxies.

In summary, using the $(\text{NUV} - r^+)_{\text{corr}}$ vs. redshift diagram, we classify galaxies in the COSMOS field into three subsamples, with 10,493 red, 2,347 green and 25,996 blue galaxies, respectively. We divide our sample into 8 redshift bins with bin size $\Delta z = 0.1$ within the redshift range of $z = [0.2, 1.0]$. In each redshift bin, a low mass limit M_{lim} was set to reduce the bias of faint galaxies. The information of our sample is summarized in Table 1.

3.2. Comparison sample

Next, the properties of green galaxies are compared with those of red and blue galaxies. To ensure that the differences shown in the comparisons are driven by different star formation properties of different samples, but not driven by their different mass distributions, red and blue comparison samples were made with similar stellar mass distributions as that of the green sample. For a green galaxy with stellar mass M_0 and redshift z_0 , matched galaxies from red or blue samples were initially chosen. The matched galaxy meets stellar mass $|M_* - M_0| < 0.10$ dex at the redshift slice of $|z - z_0| < 0.02(1 + z_0)$, where M_* and z are stellar mass and redshift of the matched galaxy, respectively. Given that there are few blue galaxies with stellar mass $\log(M_*/M_\odot) > 11.0$, the upper mass limit of green galaxies was set to $\log(M_*/M_\odot) = 11.0$. The number of matched galaxies (N_{match}) depends on M_0 and z_0 . About 98% green galaxies have $N_{\text{match}} > 15$ in both the red and blue samples. A galaxy was then randomly selected from the matched sample for comparison of physical properties with the green galaxy. Thus for a green galaxy sample selected from a certain redshift bin, a blue or red comparison sample with the same size and mass distribution was prepared. This procedure eliminated the selection effect in the subsequent comparisons.

4. RESULTS

4.1. Morphology

We cross-matched our galaxy sample with the ZEST catalog, with an angular diameter of $D = 3.0''$. The median separation value of the first closest counterpart is about $0.2''$. Then, a proper separation distance, $D_{\text{separate}} < 0.5''$, is chosen. Considering that the ZEST catalog covers a smaller area ($\approx 1.6 \text{ deg}^2$) compared with the photometric catalog ($\approx 2 \text{ deg}^2$), our final sample contains $\approx 25,000$ galaxies with ZEST morphological classifications.

4.1.1. The (Gini–Asymmetry) and (M_{20} –Gini) diagrams

Many previous studies found ETGs and LTGs are roughly separable on Gini coefficient G and asymmetry parameter A diagram (Abraham et al. 1996; Lotz et al. 2004; Kong et al. 2009). More information of the parameter definition can be found in Conselice et al. (2000) and Glasser (1962). Briefly, ETGs have compact cores and regular surface brightness distributions, thus have high G and low A values. For LTGs the situation is opposite. Galaxies can be roughly classified as early-types, late-types or irregular types based on their locations on the (G – A) plane (Capak et al. 2007b).

The $G-A$ diagrams of both green and comparison samples are plotted in Figure 4. A total of 15 blue and 15 red comparison samples were used. The blue and red contours show the G and A distributions of blue and red comparison samples, respectively. Red galaxies have high G and low A values, indicating that they are compact and have regular surface brightness distributions. Indeed most red galaxies are classified as early-type (E+S0) or early-type spirals. Conversely, blue galaxies have low G and high A values and are mostly classified as disk or irregular galaxies. The bulk of blue and red galaxies are located in different regions on the $G-A$ plane, but some blue and red galaxies have similar G and A values, and reside in the joint regions. Interestingly, green galaxies are mostly distributed in the joint regions. The average G and A values of green galaxies are also between those of blue and red galaxies at each redshift bin. Note that our sample spans a redshift range of $z = [0.2, 1.0]$. The ACS i_{814w} band corresponds to 4000-6700 angstrom in the rest-frame within this redshift range. It has been shown that the morphological K-correction within this wavelength range is small (Lotz et al. 2004), and the ZEST classifications are still robust (Bundy et al. 2010).

Figure 5 shows the M_{20} parameter vs. the Gini coefficient diagram. This diagram can also effectively classify galaxies into early-types or late-types (Lotz et al. 2006; Kong et al. 2009; Wang et al. 2012). To illustrate the robustness of morphological classification using Gini and M_{20} , we show some randomly selected galaxies on the $(G-M_{20})$ plane. The symbols are replaced by *HST/ACS* images (Figure 6). Generally, red quiescent galaxies with high G and low M_{20} values have spheroidal morphologies, whereas blue star-forming galaxies with low G and high M_{20} values have disk-like morphologies. Visually inspection of green galaxy images in Figure 6 suggests that most green galaxies have prominent bulges and significant disk components. Our findings are in agreement with those of Balogh et al. (2011) and Mendez et al. (2011), that is, green galaxies are mostly at the morphologically transiting stage between blue and red galaxies.

4.1.2. Bulgeness

This subsection investigates the bulge properties of disk galaxies ($T_{\text{ZEST}}=2$). Disk galaxies compromise approximately 75% of the total galaxies. The ZEST morphological classification assigns disk galaxies in 4 bins according to their bulge-to-disk ratio, which is described as the bulgeness parameter B_{ZEST} . Since it is hard to fully separate galaxies into different types using bivariate distributions such as Figure 4 and Figure 5, the bulgeness parameter allows one to investigate the morphologies of green galaxies in more detail.

Figure 7 shows the fractions of red, blue and green disk galaxies with different B_{ZEST} parameter as a function of redshift. The green galaxies were categorized into two subsamples according to their stellar mass. Only the results of low mass galaxies at $z < 0.7$ were shown in the figure

because there are few low mass green galaxies at high redshift. The error bars were derived as the standard deviations from 15 red and blue comparison samples. For green galaxies, the error bars were computed by 1000 bootstrap resamplings. More information can be found in Table 2.

In the high mass bin, red galaxies are mainly composed by $B_{\text{ZEST}}=0$ and $B_{\text{ZEST}}=1$ type, accounting for about 85% to 95%. The fractions of these two types also show very strong redshift evolution since $z \approx 0.7$. Our findings are in good agreement with Bundy et al. (2010) (see Figure. 3 of Bundy et al. 2010), suggesting that $\log(M_*/M_\odot)=[10.0,11.0]$ red sequence disk galaxies are more bulge-dominated and abundant since $z \approx 0.7$. Note that there are rare red pure disk galaxies within this mass range. Blue galaxies show much stable B_{ZEST} and mild redshift evolution. The fraction of blue pure disks decreases since $z \approx 0.7$. The fraction of green galaxies classified as $B_{\text{ZEST}}=0$ is significantly lower than that of red sequence galaxies, indicating that most of them still contain significant disk components. The jump at $z = 0.25$ may due to the small sample size ($N=26$) at the redshift bin. Only 5% to 10% green disk galaxies are classified as pure disk systems.

Galaxies with $\log(M_*/M_\odot) < 10.0$ have very different B_{ZEST} , in that nearly no bulge-dominated galaxies are present within this mass range for all three samples. The B_{ZEST} of low mass red disks shows no redshift evolution. However, the fraction of blue pure disk galaxies decreases from 45% at $z \approx 0.65$ to 20% at $z \approx 0.25$. The B_{ZEST} evolution trends of green galaxies and red galaxies are similar. The most striking feature is that, even at lower mass, the fraction of green pure disk systems and red galaxies are similar.

In summary, the fraction of green galaxies classified as $B_{\text{ZEST}}=0$ and $B_{\text{ZEST}}=1$ is significantly higher than that of star-forming galaxies, and the fraction classified as $B_{\text{ZEST}}=3$ is only about 5% to 10%. Compared with red galaxies, most green galaxies still have significant disk components, which implies that green disks are also at an intermediate stage between blue and red disks. The lack of green pure disk galaxies suggests that the suppression of star formation activities may be connected with galaxy bulge formation. Considering the great B_{ZEST} differences between green and blue galaxies, we disfavor the scenario that green galaxies are simply faded blue galaxies.

4.1.3. Compare with the Mixed Sample

In the above two subsections, the morphological parameters of green galaxies are found to be intermediate between those of red and blue galaxies. However, it is still not clear whether green galaxies form a distinct population, or their observed morphological properties can be explained by a simple mix of blue and red galaxies. To answer this question, the morphological parameters of green galaxies are compared with those of the “mixed” sample. As the morphologies of blue and red galaxies significantly differ from each other, the morphological parameter distributions of

the “mixed” samples depend on the ratio of blue to red galaxies ($N_{\text{blue}}/N_{\text{red}}$).

This part of this paper explains the process of creating a combined “mixed” sample, with fixed blue to red ratio of $N_{\text{blue}}/N_{\text{red}} = P/(1 - P)$, where $P \in (0, 1)$. Firstly, for a green galaxy which with stellar mass M_0 and redshift z_0 , a blue-matched sample and a red-matched sample were formed. This was done to meet the required stellar mass $|M_* - M_0| < 0.10$ dex at the redshift slice of $|z - z_0| < 0.02(1 + z_0)$, where M_* and z are stellar mass and redshift of the matched galaxy, respectively. Then we generate a uniform random number r_0 between 0.0 and 1.0. When $r_0 \leq P$, we randomly select a galaxy from the blue-matched sample, otherwise we select a galaxy from the red-matched sample, to form the “mixed” sample. A combined blue and red galaxy sample with fixed blue to red ratio was thus formed. This procedure also assures the “mixed” sample and the green sample are matched in mass and redshift.

The $G-A$ diagram of the green and “mixed” samples is shown in Figure 8. The green galaxies were divided into 4 redshift bins, from which mixed samples with 5 different blue-to-red ratios were created. In each panel, 15 different mixed samples were used to minimize the random disturbance. As shown in Figure 8, low $N_{\text{blue}}/N_{\text{red}}$ yields low average A and high G values, and the trend is reverse at high $N_{\text{blue}}/N_{\text{red}}$ ratios. Green galaxies have similar average A value with the “mixed” samples when $N_{\text{blue}}/N_{\text{red}} = 0.2/0.8$, whereas the average G value is significantly lower. The most reasonable compromise of average A and G values between green and “mixed” samples is observed when $N_{\text{blue}}/N_{\text{red}}$ is around 1.0. However, it is clear that the G scatters in green sample are *significantly smaller* than those of the “mixed” samples, as shown in the three middle rows across all redshift range. Green low G systems have low A values, which means that they are more regular than those with similar G values in the “mixed” samples. Therefore, a simple combination of blue and red galaxies cannot reproduce the morphological properties of green galaxies.

Using different method, Mendez et al. (2011) also demonstrated that green morphological parameter distributions are statistically different (at 2σ level) from those of the simple mix of blue and red galaxies. Our finding is consistent with that presented by Mendez et al. (2011). Thus green galaxies most likely form a distinct population, but this phenomenon is not due to selection effects.

4.2. Spectral Analysis

4.2.1. Average Spectra of Galaxies

The zCOSMOS provides about 10,000 galaxy spectra down to $i^+ = 22.5$, facilitating the further exploration of spectral characteristics of green galaxies. However, most of the spectra have very low signal-to-noise ratio (S/N) and are difficult to be analyzed individually. To obtain a higher S/N ratio, an average spectrum for each subsample was created by stacking method (Eisenstein et

al. 2003; Shiyon 2007; Chen et al. 2009; Shu et al. 2012).

Next, the photometric catalog was cross-matched with the zCOSMOS spectroscopic sample using a $1.0''$ angular diameter, from which a sample containing about 550 green galaxies, 1800 red galaxies and 6000 blue galaxies was generated. The sample was divided into two redshift bins, $z = [0.2, 0.5]$ and $z = [0.5, 1.0]$. There are few blue galaxies with stellar mass $M_* > 10^{11.0} M_\odot$, and at $z > 0.5$ most red and green galaxies have stellar mass $M_* > 10^{10.5} M_\odot$. Hence, a mass range of $\log(M_*/M_\odot) = [10.0, 11.0]$ for $z = [0.2, 0.5]$, and $\log(M_*/M_\odot) = [10.5, 11.0]$ for $z = [0.5, 1.0]$ was chosen. Blue galaxies have low M/L ratio and dominate the low mass end in a flux-limited sample, which means that a direct stacking without weight for blue sample mostly reflects the signatures of low mass galaxies. For red sample the situation is just reversed. To create average spectra with a same mass distribution, galaxies were weighted as a function of mass and redshift for each subsample. We determine the number of galaxies within mass and redshift bins (at the low redshift bin, $\Delta \log(M_*)=0.34$; at the high redshift bin, $\Delta \log(M_*)=0.25$; redshift bin size is $\Delta z = 0.1$) both in the full sample and in each subsample. We then weigh each spectrum by the number of the full sample divided by the number in the subsample. This procedure allows the breaking of mass dependence.

The average spectra of red, green and blue galaxies are shown in Figure 9. In the low redshift bin, the average spectra range from 4600 to 6700 Å, and are normalized to the average flux between 5050 Å and 5100 Å. In the high redshift bin, the spectra are showed at shorter wavelength, including the [O II] lines. Each average spectrum is stacked by more than 100 individual spectra (except the green sample in the low redshift bin). Given that the mass dependence has been minimized in the stacking procedure, these average spectra can be treated as the “representative spectra” of each subsample.

The red average spectra are dominated by absorption lines. The emission lines reflecting (directly or indirectly) star formation activities, such as $H\alpha$ and [O II] are rare in the red spectra. The strong jump at 4000 Å and very strong Ca H+K absorption lines demonstrate that red galaxies are dominated by old stellar populations. The metal lines, such as the Mgb and the G-band absorption lines are most remarkable in the red spectra. Briefly, the red average spectra are typical quiescent galaxy spectra. There are strong emission lines in the blue spectra. The strong [O II], $H\alpha$ and $H\beta$ emission lines demonstrate that blue galaxies are still at active stage and forming stars.

Interestingly, the green spectra are significantly different from the red and blue ones. The [O II], $H\alpha$ and $H\beta$ emission lines are still visible, but obviously much weaker than those of star-forming galaxies. Specifically, the [O III] / $H\beta$ ratios of green spectra are higher than those of blue spectra, confirming the result of Coil et al. (2008). However, in the low redshift bin, we find the [N II] $\lambda 6583/H\alpha$ ratio of the green spectrum is still significantly lower than that of a typical AGN. The continua of green spectra are much similar with those of red galaxies. Specifically, the 4000

Å break of green galaxies is between the blue and red ones, indicating that the average stellar age of green galaxies is between the ages of the red and blue ones.

4.2.2. SFH from the average spectra

The high S/N average spectra allow the extraction of galaxy star formation history (SFH) information by comparing them with stellar population synthesis models. This is done by comparing the average spectra in the $z=[0.5,1.0]$ bin with the STARLIGHT. ² STARLIGHT aims at fitting an observed spectrum with a linear combination of theoretical simple stellar populations (SSPs). The model spectrum of STARLIGHT is given by:

$$M_\lambda = M_{\lambda_0} \left(\sum_{j=1}^N x_j b_{j,\lambda} r_\lambda \right) \otimes G(v_*, \sigma_*), \quad (2)$$

where M_λ is the model spectrum, M_{λ_0} is the synthesis flux at the normalization wavelength λ_0 , x_j is the so-called stellar population vector, $b_{j,\lambda}$ is the j th SSP spectrum at λ , and $r_\lambda \equiv 10^{-0.4(A_\lambda - A_{\lambda_0})}$ represents the reddening term. The $G(v_*, \sigma_*)$ is the line-of-sight stellar motions which are modeled by a Gaussian distribution centered at velocity v_* and with a dispersion of σ_* . N is the total number of SSP models. In our work, the SSP base consisted of $N = 126$ SSPs, with 6 metallicities ($Z = 0.005Z_\odot, 0.02Z_\odot, 0.2Z_\odot, 0.4Z_\odot, Z_\odot$ and $2.5Z_\odot$) and 21 ages (from 1 Myr to 7.5 Gyr), which were taken from evolutionary models in BC03. The maximum age corresponded to the cosmic age at $z=0.5$. The galactic extinction law of Cardelli, Clayton & Mathis (1989) with $R_V = 3.1$ was adopted. Emission lines were masked in the fitting procedure. The STARLIGHT produced the SSP fraction, dust attenuation A_V , velocity dispersion σ , and stellar mass M_* . Following Cid Fernandes et al. (2005), the flux- and mass-weighted average ages are defined, which are respectively defined as:

$$\langle \log t_* \rangle_L = \sum_{j=1}^N x_j \log t_j; \quad \langle \log t_* \rangle_M = \sum_{j=1}^N u_j \log t_j, \quad (3)$$

where x_j is the flux-weighted population vector (i.e., the fraction of flux contributed by certain SSP), and u_j is the mass-weighted population vector. The average metallicities $\langle Z_L \rangle$ and $\langle Z_M \rangle$ can be derived in a similar way.

The STARLIGHT best-fit spectra as well as the SSP stellar population vectors are presented in Figure 10. only the high redshift average spectra were fitted because the spectra at low redshift bin did not include the 4000 Å break, which was especially important for constraining the stellar

²www.starlight.ufsc.br

age. Spectra were fitted up to $\lambda = 4900 \text{ \AA}$ since when $z \approx 1$ spectra were de-redshifted to $\lambda < 4900 \text{ \AA}$ in the rest-frame. As demonstrated by Figure 10, the combination of SSP spectra fits the average spectra very well. It is worth noting that the individual output vector may be dramatically deviated from the simulated input value. However, the average values of age and metallicity should be more reliable, whatever they are weighted by flux or mass. The average flux-weighted ages are 3.92, 1.81 and 1.15 Gyr for red, green and blue spectra, respectively. A similar trend still exists when weighted in mass. The average metallicity also shows a clear trend, wherein red galaxies are the most metal-rich and blue galaxies are metal-poor.

The distributions of the SSP vectors are also interesting. The red spectra show very weak emission lines and should be dominated by old stellar populations. Interestingly, the flux-weighted vectors also show that there is no contribution of young stellar populations ($< 0.3 \text{ Gyr}$) in red spectrum. The contributions of old stellar populations ($> 6.25 \text{ Gyr}$) reach about 40%. For the green spectrum, the fraction of old populations is significantly smaller than the red one. For the blue spectrum, there is a significant fraction ($\sim 20\%$) of very young stellar populations ($< 0.01 \text{ Gyr}$) and few old stellar populations.

4.3. Environment

This section presents an investigation of the environment of green galaxies. The projected N_{10} -nearest-neighbor surface density was adopted as local galaxy density estimator. Capak et al. (2007b) showed that the use of photometric redshift can also correctly characterize galaxy density in the COSMOS field. To be consistent with previous studies (Capak et al. 2007b; Ideue et al. 2012), the 10th nearest neighbor was used in our analysis. The local galaxy density was calculated as $\Sigma_{10} = 11/(\pi D_{p,10}^2)$, where $D_{p,10}$ (in Mpc) is the projected proper distance to the 10th nearest neighbor. The projected densities was computed using $i^+ < 24.0$ galaxies. A redshift slice centering on each galaxy with $\pm \Delta z = 0.033(1+z)$ was used, corresponding to $\pm 3\sigma_{\text{photo}z}$, where z is the redshift of central galaxy. Galaxies located near the mask regions or survey edge were excluded from statistic. To check the reliability of the density estimator, the sample was cross-matched with the released COSMOS field X-ray group catalog (George et al. 2011). The results show that the X-ray group members (which have group member likelihood $P_{\text{mem}} \geq 0.5$) mostly locate at the high Σ_{10} end at each redshift bin.

Figure 11 shows the Σ_{10} histograms for blue, green and red galaxies indicated as blue solid, green filled and red solid lines, respectively. The Σ_{10} distributions were averaged over 15 different comparison samples. The error bars in the figure show the standard deviations of the 15 different comparison samples. In addition, the Σ_{10} histograms for the $z < 1.0$ X-ray group members were plotted (shown as black shaded histograms). The global Σ_{10} at low redshift is higher than that

at high redshift, due to galaxy density evolution and flux limit for observation. The Σ_{10} was not normalized relative to the median galaxy density at each redshift bin. Blue galaxies always prefer to reside in less dense environments, as shown in Figure 11. Conversely, red galaxies are preferentially found in dense environments. Group members dominate the high density end at each redshift bin as expected. However, the environmental diversities of blue and red galaxies decreases with increasing redshift. This can be attributed to the different galaxy composition in dense environments at different redshifts. At low redshift, galaxies in groups or clusters are mainly red and quiescent. However, at high redshift, a large fraction of group members still form stars and with blue colors. This is first reported in Butcher & Oemler (1978), which is called the “B-O” effects.

The cumulative distribution curve of each sample is shown below the histogram panel. At $z < 0.7$, green galaxies and red galaxies have similar Σ_{10} distributions, as shown in Figure 11. Compared with blue galaxies, there is a larger fraction of green galaxies residing in dense regions, especially at $z < 0.5$. However, in all panels at $z > 0.7$, green galaxies and blue galaxies have similar Σ_{10} distributions. In some redshift bins, the differences between the three cumulative lines are very subtle, which may not be sufficient to conclude that the Σ_{10} distributions of these subsamples are statistically different. However, the consistent Σ_{10} trend for green galaxies at $z < 0.7$ suggests that the environment effects may play a more important role in the formation of this population at subsequent cosmic epoch.

To investigate the environment dependence on stellar mass, the green galaxy sample was divided into two mass bins at $z < 0.7$: $\log(M_*/M_\odot) = [10.0, 11.0]$ and $\log(M_*/M_\odot) < 10.0$. The Σ_{10} distributions of the binned samples are shown in Figure 12. Interestingly, the Σ_{10} distributions of red and green galaxies remarkably differ from those of blue galaxies in the low mass bin: *In comparison with blue samples, red and green samples have larger fractions of galaxies residing in dense environments.*

However, the remarkable density distribution differences among these three subsamples shown in the low mass bin are diluted in the high mass bin. To show the Σ_{10} distribution differences more statistically, we extend the Kolmogorov-Smirnoff (KS) tests to the three distributions and summarize the results in Table 3. The result of KS test gives small probabilities (< 1 percent) that the Σ_{10} of green and blue galaxies are drawn from the same distribution at $z < 0.5$ when $\log(M_*/M_\odot) < 10.0$. For the $\log(M_*/M_\odot) = [10.0, 11]$ bin, the KS test gives larger probabilities, in good agreement with visual inspection.

In summary, green galaxies at $z > 0.7$ have similar Σ_{10} distributions with those of star-forming galaxies. At lower redshift, low mass green galaxies have similar Σ_{10} distributions with those of quiescent galaxies; they preferentially reside in dense environments, especially at $z < 0.5$. Our findings suggest that environmental effects may be crucial for quenching star formation activities

in $\log(M_*/M_\odot) < 10.0$ galaxies at $z < 0.7$. For more massive galaxies, quenching does not show evident dependence on galaxy local environment.

5. Discussion

5.1. The nature of green valley galaxies

In the above analysis green galaxies are found to have significantly different morphological and spectral characteristics with respect to blue and red galaxies. Their morphological properties cannot be produced by a simple mix of blue and red galaxies, and they most likely form a distinct population. This subsection discusses the components of the green population.

The simplest explanation for the presence of green galaxies is that they are transiting galaxies, which are fading original star formation, on the way towards the red sequence. The transiting scenario is required to explain the observed redshift evolution in stellar mass functions for star-forming and quiescent populations. Some properties of green galaxies, such as the average Gini coefficient, the bulgeness parameter and the stacked emission lines, are intermediate between those of blue and red galaxies. These results can be expected if green galaxies are at the transiting stage.

However, there are other possible ways to explain the existence of green galaxies. One possible explanation is that green galaxies are rejuvenated red galaxies. Red galaxies obtain gas supply either from gas-rich minor merger or from gradual accretion, then start low level star formation activity and return to the GV. They might move to red sequence again after the gas is exhausted. This scenario is supported by the observation of ETGs in the FUV and NUV bands, which reveals that a considerable fraction (about 15% to 30%) of ETGs have low level recent star formation activities. Many studies favored the scenario that the star formation in ETGs are triggered in hitherto quiescent galaxies. Such phenomenon is termed “rejuvenation” in the literature (Rampazzo et al. 2007; Thomas et al. 2010; Thilker et al. 2010; Marino et al. 2011). It is important to evaluate the proportion of these sources in GV. Fang et al. (2012) studied the extended star-forming early-type galaxies (ESF-ETGs) in low redshift GV and estimated that $\approx 13\%$ GV galaxies have similar UV-optical color and stellar mass with those of ESF-ETG candidates. Another possible explanation is that galaxies are relatively stationary in the GV because of inefficient star formation. In this picture, galaxies will keep low level star formation for very long periods of time due to quasi-static gas accretion from inter-galactic medium (IGM) and never reach true passivity (Salim et al. 2012). This so-called “incomplete quenching” phenomenon could be also possibly related to “morphology quenching” as demonstrated in Martig et al. (2009). In this scenario, after the cold stream fuel star formation shut down, the further fragmentation of gaseous disks (e.g., the ability to form stars) can be suppressed by deepening central potential well or the declining self-gravity of the gas. This

model predicts large bulges and slow quenching in disks.

About 20% green galaxies are classified as ETGs with ZEST. Assuming all these ETGs are "rejuvenated" red galaxies, they would only occupy a small fraction of the entire green sample. In Figure 6 and Figure 7 we find the majority of green galaxies host bulge components as well as significant disks. Their significant disk components are more possibly inherent rather than having formed from later gas accretion. It is difficult to distinguish those green galaxies due to "incomplete quenching", which prevents an accurate proportional estimation. Nevertheless, galaxies of this category should not be dominant in GV because they are expected to stay in GV for long periods of time, which makes it difficult to explain the color bimodality. In summary, the observed properties of green galaxies are consistent with the transiting scenario. A modest proportion of green galaxies might have different origins and evolutionary paths.

5.2. Comparison with previous studies

In this paper, GV was defined using dust-corrected $\text{NUV}-r^+$ color. Because the dust-corrected $\text{NUV}-r^+$ color is a good tracer of sSFR, in the current paper GV is equivalent to an intermediate sSFR ($\log(\text{sSFR}) \sim -10.5$). In some previous studies, GV is defined using optical color index such as $U-B$ or $U-V$. Since neither $U-B$ nor $U-V$ is sensitive to intermediate sSFR, GV galaxies defined using intermediate sSFR will degenerate with red sequence galaxies in the $U-B$ or $U-V$ CMD. We have investigated the $U-B$ selected GV galaxies using the criterion of Mendez et al. (2011) and found, on the one hand, about 75% of them have $\log(\text{sSFR}) > -10.0$, and only about 20% of them have $\log(\text{sSFR}) = [-10.0, -11.0]$. On the other hand, we found about 45% $\log(\text{sSFR}) = [-10.0, -11.0]$ galaxies are degenerated with red sequence galaxies in the M_B versus $U-B$ diagram. One should know the differences between optical color and sSFR GV selections when comparing our works with others.

Mendez et al. (2011) studied morphologies of ≈ 300 green galaxies in the AEGIS field within the redshift range of $z = [0.4, 1.2]$. They showed that green galaxies are generally massive ($\sim 10^{10.5} M_\odot$) disk galaxies with high concentrations. The findings of Mendez et al. (2011) are confirmed by the current work based on a larger green galaxy sample selected from similar redshift range. Thanks to the large green galaxy sample, the morphology of less massive $M_* < 10^{10.0} M_\odot$ green galaxies were also investigated. These less massive green galaxies do not show significant increase in their concentration since $z \approx 0.7$.

We also found that green galaxies have high $[\text{O III}]/\text{H}\beta$ ratio as reported in Coil et al. (2008). Coil et al. (2008) interpreted this as more AGN activity in green galaxies as compared with blue galaxies. The samples of Coil et al. (2008) were selected from the DEEP2 survey and mainly

covered the redshift range of $z = [0.7, 1.5]$. For the galaxies at $z = [0.2, 0.5]$, the [N II] $\lambda 6583$ and $H\alpha$ emission lines are showed. As shown in Figure 9, the [N II] $\lambda 6583/H\alpha$ ratio of a typical green galaxy is significantly higher than that of a blue galaxy, yet it is still lower than a typical Seyfert galaxy (Kauffmann et al. 2003b). Therefore, in this work, a typical green galaxy will be classified into the “transition” class, using the BPT diagram (Baldwin et al. 1981).

Coil et al. (2008) found that green galaxies have similar clustering amplitude at a small scale ($< 1\text{Mpc}$) as compared with blue galaxies, whereas at larger scales green galaxies show clustering amplitude that is close to that of red galaxies. Coil et al. (2008) explained that green galaxies are residing in the same dark matter halo as red galaxies, but are mainly spread in the outskirts. Galaxy properties are expected to correlate with the parent dark matter halo, inside which densities are evaluated on scales comparable with a typical viral radius ($\sim 1\text{Mpc}$). Figure 11 shows that green galaxies at $z > 0.7$ have similar Σ_{10} distributions with blue galaxies. In comparison with red galaxies, green galaxies tend to prefer lower density environments, which is also in agreement with the findings of Coil et al. (2008). Balogh et al. (2011) reported the existence of a large green population in X-ray group. We will compare our results with those of Balogh et al. (2011) and discuss in detail in Section 5.5.

5.3. Quenching connected with bulge formation

About 90% of green disk galaxies have bulge components. Specially, the fraction with prominent bulge is about 60% to 70% in the green disk sample, and only $\approx 35\%$ in the blue disk sample. *The presence of bulge in the majority of green galaxies suggests that star formation quenching in this population possibly accompanies or has connection with bulge formation.*

Recent studies have found that quiescent galaxies are mostly associated with the presence of bulges. Bundy et al. (2010) found that passive disks typically have Sa–Sb morphological types and large bulges, based on the COSMOS data; Kauffmann et al. (2012) found there are clear thresholds in bulge-to-disc ratio and in stellar surface density that demarcate the location of quiescent galaxies. They proposed that the processes associated with bulge formation play an important role in depleting the gas in galaxies; Bell et al. (2012) studied a sample from CANDELS and found that most quiescent galaxies host prominent bulges, and many of them have significant disks. They argued a prominent bulge (and perhaps associating with a supermassive black hole) is an important condition for quenching star formation on galactic scale over the last 10 Gyr. Our findings confirm that both green and red galaxies tend to have prominent bulges.

Cheung et al. (2012) searched for traces of possible quenching processes through galaxy structural parameters and found the central surface stellar mass density best discriminates between red

sequence and blue cloud. They found that red sequence bulges are roughly twice as massive as blue cloud bulges at the same stellar mass. Their results suggest that the innermost structure of galaxies is most physically linked with quenching. Some possible quenching mechanisms are discussed in Cheung et al. (2012). However, the ways by which these mechanisms relate to bulge-buildup is still unclear.

The current study finds that a small fraction (about 5% to 10%) of green disk galaxies does not harbor identified bulge components. This finding is consistent with that of Mendez et al. (2011), who reported that 12% of their green galaxies have $B/T=0$. We stress that there is no clear boundary separating green and blue galaxies in the morphological parameter planes. These bulgeless green disks must have their star formation suppressed by other mechanisms without forming galactic bulges.

5.4. Quenching connected with AGNs

There are some recent indications that active galactic nucleus (AGN) inhabits GV, both from X-ray surveys (Nandra et al. 2007; Coil et al. 2009) and optical line-ratio diagnostics (Salim et al. 2007). However, it is still unclear whether there are direct relations between AGNs and star formation quenching process in green galaxies. On the one hand, some studies found observational evidence that a powerful AGN can drive high speed outflow expelling the interstellar mediums, and will suppress the star formation of its host galaxy in a very short period of cosmic time (Feruglio et al. 2010; Sturm et al. 2011; Page et al. 2012). On the other hand, studies based on large samples reported that AGNs have complicate relations with star formation activities, but may not be directly responsible for quenching star formation (Bundy et al. 2008; Alonso-Herrero et al. 2008; Aird et al. 2012). Until now, despite recent progress, how AGNs regulate the star formation and shape galaxy global properties is a highly debatable.

To understand the role of AGN feedback, it is important to compare the properties of AGN host galaxies with those of inactive galaxies. While considering the fact that when a galaxy hosts an AGN, its observed SED is a superposition of an AGN and the host component. Thus one must subtract the AGN contribution from the total observed flux before deriving the correct color and mass of the host galaxy. Studying the link between AGNs and their hosts is a key question in astrophysics. However, this is beyond the scope of the current work. In this paper, we will just briefly discuss the recent progresses in this field.

Xue et al. (2010) found moderate-luminosity AGN hosts apparent no color bimodality on the CMD. When matched in mass, AGN hosts lie in the same region on the CMD as inactive galaxies. They suggested that the presence of moderate-luminosity AGN activity does not have a

significant effect on the galaxy color. Bongiorno et al. (2012) explored the host galaxy properties of ≈ 1700 AGNs in the COSMOS field, and found AGN hosts are mainly massive, red galaxies. They found no conclusive evidence suggesting that AGNs have powerful influence on the star-forming properties of their host galaxies. Rosario et al. (2013a) studied the properties of X-ray selected AGN hosts in the Cosmic Assembly Near-IR Deep Legacy Survey and found, the colors, color gradients and stellar population properties of AGN hosts are similar with those of inactive galaxies with the same stellar mass. However, in a most recent study, using far-infrared observations of the two Chandra Deep Fields, Rosario et al. (2013b) found the UV-to-optical colors of AGNs are consistent with equally massive inactive galaxies at same redshift, whereas their FIR distributions are statistically similar with those of star-forming galaxies.

Understanding the importance of AGN feedback requires a complete AGN sample spanning a wide luminosity range. The AGN samples used in previous studies are selected by X-ray, spectral indices or IR SEDs. As suggested in many previous studies, a significant fraction of obscured AGNs will not be identified in insufficient deep X-ray surveys. The IR AGN selection criteria are relatively insensitive to dust obscuration. However, as suggested in Mendez et al. (2013), the IR selection appears to be biased in selecting high luminosity AGNs. We have used the mid-IR AGN selection criteria from Donley et al. (2012) to select AGNs from our galaxy sample. 90 AGNs were selected with the IRAC photometry, and most of them are blue. However, this must be a small fraction of the actual number, which is likely owing to the relatively more shallower photometry in IRAC bands with respect to the optical bands. To summary, whether AGN feedback is responsible for quenching cannot be well constrained in our study.

5.5. Quenching connected with environmental effects

Galaxies in dense regions are influenced by environmental conditions, such as galaxy interactions, tidal forces due to the cumulative effect of many weaker encounters, and gas stripping due to the interaction with IGM, which can affect (more or less) their evolutionary paths. A great deal of works support that the dense environments are especially important for gas stripping/removal in LTGs and turning them into ETGs (Boselli & Gavazzi 2006; Cooper et al. 2006; van den Bosch et al. 2008; Smith et al. 2010; van der Wel et al. 2010; Weinmann et al. 2010).

Our findings show that green galaxies exist in various environments, indicating that environmental effect is not the sole explanation responsible for quenching star formation in this population. In Section 4.1.2, most green disks are found to host significant bulges as well as disk components. These green disks are likely the progenitors of S0 or passive spirals. Bundy et al. (2010) found that passive spirals in the COSMOS field harbor large bulges, but not confined to dense environments. However, less massive green galaxies ($M_* < 10^{10.0} M_\odot$) at $z < 0.7$ prefer

dense environments, strongly suggests that the environmental conditions may play an important role on quenching at the later cosmic time.

Although both the morphological evolution (Kováč et al. 2010) and star formation activity are influenced by environment, the dominated mechanism affecting galaxy evolution in dense environments is still debatable. Because there are only 1-2 clusters in the COSMOS field, strong ram pressure stripping, which works in cluster cores, will not play a dominant role in quenching in this study. In a group environment, frequent galaxy interactions are expected to be especially efficient in influencing galaxy evolution. Tidal interactions can trigger star formation (Lambas et al. 2003; Nikolic et al. 2004; Li et al. 2008), which could be a factor in the transformation of blue, star-forming galaxies to red, quiescent galaxies. (Kenneth et al. 2011; Patton et al. 2011).

Comparing the merger rate between blue, green and red galaxies may be helpful in assessing the role of merger on the formation of green galaxies. However, accurate measurement of merger fraction requires spectroscopic redshifts and very high sampling rate. The zCOSMOS survey has low sampling rate (< 0.1) for galaxies with close companions ($D_{\text{separation}} < 5.0''$), which restricts an accurate merger rate measurement. We note that the ways by which mergers shape galaxy properties have been widely discussed in literature. Perez et al. (2009) suggested that, at intermediate densities, close pairs could have experience more rapid transition onto the red sequence than isolated galaxies. Ellison et al. (2010) found that there is a clear enhancement of bulge/total ratio (B/T) when pairs have small separations ($< 30 h^{-1}$ kpc). They interpreted this as the signature of central star formation in interacting pairs. Mendez et al. (2011) found most green galaxies in the AEGIS field are not classified as mergers, and their merger rate is even lower than that of blue galaxies. Alonso et al. (2012) studied galaxy pairs in SDSS groups and found, the CMD of groups/clusters pairs consists of a clear excess of extremely blue and red galaxies with respect to that of the control sample. Most of these studies suggest that mergers enhance star formation activities, and the interacting galaxies evolve more rapidly than their isolated counterparts. If this is the case, then the interacting galaxies will pass their GV phase in a shorter time than isolated galaxies. Thus, the results shown in Mendez et al. (2011) and Alonso et al. (2012) are natural.

In galaxy groups, very weak ram pressure can strip gas, thereby gradually shutting off star formation. This process is known as “strangulation”. “Harassment”, which is known as the cumulative effects of many weak encounters and tidal interactions, also works in a group environment. These two mechanisms are thought to be especially important to the evolution of low mass galaxies (Barazza et al. 2002; Haines et al. 2006, 2008). As Compared with merger or strong galaxy-galaxy interactions, strangulation and harassment mainly act on gas content and will not modify galaxy structure directly. Violent merging of two spiral galaxies is most likely to produce a bulge-dominated ETG. Simulations have showed that the remnants of strangulation should have similar structures with those of disk galaxies (McCathy et al. 2008), which may help in interpreting the

existence of bulgeless green disks. The lack of low mass bulge-dominated systems in both red and green disks (see Figure 7) suggests that, in a group environment, strangulation and harassment are the most likely mechanisms responsible for quenching.

The current study find that green galaxies reside in similar density environments as blue galaxies at $z > 0.7$. Balogh et al. (2011) targeted 7 galaxy groups in the COSMOS field and claimed that they discovered a large fraction of transiting galaxy population in X-ray groups at $0.85 < z < 1.0$. However, their sample size is much smaller (about 100 galaxies in total, and about 20 of them are green galaxies) than ours. They used the k-corrected $(V - z)$ color index to define GV, whereas we use the dust-corrected $\text{NUV} - r^+$ color. Thus the composition of green galaxies are quite different in these two works, as also discussed in Section 5.2. In the left panel of Figure 13 we show the $(\text{NUV} - r^+)_{\text{corr}}$ and $(V - z)^{0.9}$ for galaxies at $0.8 < z < 1.0$, with the green galaxy criterion of Balogh et al. (2011) shown in vertical dashed lines. It is obvious that these two criteria select different galaxies. The GV defined by $(V - z)^{0.9}$ color is contaminated by many dusty blue galaxies. Galaxies are more efficiently separated into two main categories (blue star-forming and red quiescent) using dust-corrected $\text{NUV} - r^+$ color. In addition, our GV definition is much stricter than that of Balogh et al. (2011), which can exclude the contaminants of star-forming or quiescent galaxies more efficiently. We suggest the dust-corrected $\text{NUV} - r^+$ color should be more reliable for selecting truly transiting galaxies.

Following Balogh et al. (2011), the $(V - z)^{0.9}$ color distribution of X-ray group galaxies was compared with that of field galaxies, to check whether there was a large amount of transiting galaxies at $0.8 < z < 1.0$. The group members were selected as galaxies with $P_{\text{mem}} \geq 0.1$ in the X-ray group catalog of George et al. (2011). A low P_{mem} limit was applied in order to keep a high group member completeness. As illustrated in George et al. (2011), a $P_{\text{mem}} \geq 0.1$ member selection limit maintain 95% true group members, but brings in about 35% field contaminants. The field galaxies were selected as those residing in sparse environments (which have $\log(\Sigma_{10}) < 0.5$ and $P_{\text{mem}} = 0.0$ when cross-matched with the X-ray group catalog). The results are shown in the middle and right panels in Figure 13. As shown in Figure 13, the $(V - z)^{0.9}$ color distribution of field galaxies is very similar with that reported in Balogh et al. (2011). Given that the purity of the selected group members is about 65%, there is a need to determine if "fake" group members will distort the color distribution of "true" group members.

To do this the color distribution of "interlopers" was subtracted from that of the selected group members. The purity and completeness are formally given by:

$$p = \frac{N_{\text{selected}} - N_{\text{interlopers}}}{N_{\text{selected}}}, \quad c = \frac{N_{\text{true}} - N_{\text{missed}}}{N_{\text{true}}}, \quad (4)$$

where $N_{\text{true}} = N_{\text{selected}} + N_{\text{missed}} - N_{\text{interlopers}}$. There are 443 galaxies with $P_{\text{mem}} \geq 0.1$, thus the number of "fake" group members is about $443 \times (1 - 0.65) \simeq 155$. These 155 interlopers were assumed to

have color distributions as those of field galaxies. The $(V-z)^{0.9}$ color distribution of the interlopers-corrected group members is shown as a solid histogram in the middle panel of Figure 13. For comparison, the dust-corrected $\text{NUV}-r^+$ distribution was plotted in the right panel of Figure 13. We find that group members tend to have redder color with respect to field galaxies, whatever termed by $(V-z)^{0.9}$ or $\text{NUV}-r^+$. The $(V-z)^{0.9}$ color distribution of group member is perfectly consistent with that reported in Balogh et al. (2011). Compared with the $(V-z)^{0.9}$ color distribution of field galaxies, there is a remarkable excess of green and red galaxies located in groups at the expense of blue galaxies. The excess of galaxies residing in GV is not seen after dust correction. Most of the $M_* > 10^{10.1} M_\odot$ green galaxies defined by $(V-z)^{0.9}$ color fall in the massive star-forming category when using the dust-corrected $\text{NUV}-r^+$ classification. In summary, we successfully reproduce the results of Balogh et al. (2011). However, after dust correction, there is no excess of $M_* > 10^{10.1} M_\odot$ group galaxies residing in GV with respect to the field.

5.6. The formation of red galaxies

Previous works have suggested a significant growth of red sequence galaxies since $z \approx 1.0$. Recently, Moustakas et al. (2013) measured the evolution of stellar mass function from $z = 0-1$ using the PRIMUS and SDSS data. On the one hand, they found the space density of massive star-forming galaxies declines by 54% since $z \approx 1$. On the other hand, the most massive quiescent galaxies are largely in place since $z \approx 1$. The build-up of red sequence occurs significantly at intermediate and low mass, where they found a factor of 2-3 increase in the number density of $10^{9.5} - 10^{10} M_\odot$ galaxies since $z \approx 0.5$. In this study, our findings suggest a significant fraction of these low mass red sequence galaxies are likely quenched due to environmental effects.

We find that the build-up of red sequence is strongly mass-dependent. At $z > 0.7$, the majority of red galaxies are massive, with $\log(M_*/M_\odot) > 10.0$. Less massive galaxies join the red sequence at $z < 0.7$. The age-downsizing, according to which less massive galaxies contain younger stellar population, have been prevalently found in studies on ETGs (Thomas et al. 2005; Zhu et al. 2010; Pan et al. 2012). Some models have been proposed to explain the observation (Faber et al. 2007; Pozzetti et al. 2010). Pozzetti et al. (2010) proposed a scenario wherein intermediate-mass galaxies decrease their star formation activities to intermediate values gradually, and finally to the values similar to of those quiescent galaxies, by means of the exhaustion of either the gas reservoir or cold gas accretion, or by quenching due to AGN feedback. For the schematic of this scenario, one can refer to Figure. 21 of Pozzetti et al. (2010). In this scenario, massive star-forming galaxies have shorter quenching time scale. Finally, they evolve to red sequence on a time scale of $1 \sim 2$ Gyr, and undergo a dynamical transformation into spheroidal galaxies.

Our findings suggest that quenching relates to both mass and local density environment. How-

ever, which process (mass quenching and environment quenching) plays the dominant role is still unclear. Peng et al. (2010) have taken an empirical approach to identify how mass and environment affect the “quenching” process at different cosmic epochs. They found that the effects of mass and environment are completely separable to $z \sim 1.0$. The physical origins of environment quenching have been discussed in Section 5.5, but the actual physical mechanism leading to mass quenching remains largely unknown. Peng et al. (2010) summarized the dominant mechanism responsible for quenching as follows: at high masses ($M_* > 10^{10.5} M_\odot$), mass quenching always plays a dominant role. At lower masses, merger quenching works at $z > 0.5$ and environment quenching works at $z < 0.5$. Our results can be well explained by Peng et al. (2010) model, although the mass and redshift thresholds separating the dominant mechanism are slightly different in these two works.

6. Summary

In this paper, a sample of ≈ 2350 green galaxies was constructed using dust-corrected $\text{NUV}-r^+$ color in the COSMOS field, after which their properties were compared with those of mass-matched blue and red samples at $0.2 < z < 1.0$. The findings are summarized as follows:

1. Green galaxies mostly locate in the joint region of blue and red galaxies in the galaxy structural parameter diagrams, both on the (Gini–Asymmetry) plane and the (M_{20} –Gini) plane.

2. Red disk galaxies mostly host large or intermediate bulge components, accounting for about 80% to 90%. The fraction of green galaxies with large or intermediate bulges accounts for about 60% to 70%, which is much higher than that of blue galaxies (about 35%). Only 5% to 10% green spirals are classified as pure disk systems. Most green galaxies still harbor significant disk components.

3. The stacked spectra of green galaxies have intermediate emission lines, such as [O II], $\text{H}\beta$ and $\text{H}\alpha$. The SSP decomposition of the stacked spectra shows that green galaxies have small fraction of young stellar populations, whereas the old populations account for very large fractions. The average metallicity of green galaxies is higher than that of blue galaxies and lower than that of red galaxies.

4. The environments of green galaxies were explored using the local galaxy density Σ_{10} . At $z > 0.7$, green galaxies tend reside in similar density environment with that of blue galaxies; whereas at lower redshift, a large proportion of $M_* < 10^{10.0} M_\odot$ green galaxies reside in dense environment, which is significantly different with that of $M_* < 10^{10.0} M_\odot$ blue galaxies.

Our findings support that the physical properties of green populations are consistent with those of the transiting populations between blue star-forming galaxies and red quiescent galaxies.

We are able to reproduce the color distribution for X-ray groups members as reported in Balogh et al. (2011) at $0.8 < z < 1.0$. However, no excess of green galaxies is found in groups with respect to the field after dust-correction. Our findings support the galaxy evolution model of Peng et al. (2010).

We thank the referee for thoughtful comments and insightful suggestions that improved our paper greatly. This work is supported by the National Natural Science Foundation of China (NSFC; Nos. 11225315 and 11203023), and the Chinese Universities Scientific Fund (CUSF) and the Specialized Research Fund for the Doctoral Program of Higher Education (SRFDP; No. 20123402110037). We thank the COSMOS team to make their excellent data publicly released, Dr. Guanwen Fang and Dr. Tao Wang for valuable discussion.

REFERENCES

- Abraham, R. G., Tanvir N. R., et al., 1996, MNRAS, 279, L47
- Aird, J. et al., 2012, ApJ, 746, 90
- Alonso-Herrero, A., et al., 2008, ApJ, 677, 127
- Alonso, S., Mesa, V, Padilla, N. & Lambas, D. G., 2012, A&A, 539, 46
- Baldry, I. K., et al., 2004, ApJ, 600, 681
- Baldwin, J. A, Philips, M. M. & Terlevich R. 1981, PASP, 93, 5
- Balogh, M. L et al., 2011, MNRAS, 412, 2303
- Bell, E. L, et al., 2004, ApJ, 608, 752
- Bell, E. L, et al., 2012, ApJ, 753, 167
- Bertoldi, F., Carilli, C., Aravena, M., et al., 2007, ApJS, 172, 132
- Blanton M. R., Hogg D. W., et al. 2003, ApJ, 594, 18
- Brammer G. B., Whitaker K. E., et al, 2009, ApJ, 706, L173
- Brammer G. B, Whitaker K. E., et al, 2011, ApJ, 739, 24
- Barazza, F. D, Binggeli, B. & Jerjen H., 2002, A&A, 391, 823

- Bruzual G., Charlot S., 2003, MNRAS, 344, 1000
- Bolzonella, M. et al., 2010, A&A, 524A, 76B
- Bongiorno, A. et al., 2012, MNRAS, 427,3103
- Boselli, A. & Gavazzi G., 2006, PASP, 118, 517
- Bower, R. G et al., 2006, MNRAS, 370, 645
- Bundy, K. et al., 2008, ApJ, 681, 931
- Bundy K. et al., 2010, ApJ, 719, 1969
- Butcher H.& Oemler A. Jr., 1978, ApJ, 226, 559
- Calzetti. D, et al., 2000, ApJ, 533, 682
- Capak. P, Abraham R. et al., 2007a, ApJS, 172, 99
- Capak. P, Abraham, R. et al., 2007b, ApJS, 172, 284
- Cardelli, J. A., Clayton, G. C., Mathis, J. S., 1989, ApJ, 345, 245
- Chen Y. M, et al., 2009, MNRAS, 393, 406C
- Cheung, E, et al., 2012, ApJ, 760, 131C
- Cid Fernandes. R., Mateus, A., Sodré, L., Stasińska G., Gomes J. M., 2005, MNRAS, 358, 363
- Cluver M E, et al., 2013, ApJ, 765, 93
- Coil, A. L., et al., 2008, ApJ, 672, 153
- Coil, A. L., et al., 2009, ApJ, 701, 1484
- Conselice, C. J., Bershady, M. A. & Jangren, A. 2000, ApJ, 529, 886
- Cooper, M. C. Newman J. A., et al., 2006, MNRAS, 370, 198
- Dale, D.A. & Helou, G, 2002, ApJ, 576, 159
- da Silva, R. L ., et al., 2011, ApJ, 735, 54D
- Donley, J.L. et al., 2012, ApJ, 748, 142
- Dressler, A .et al, 1997, ApJ, 490, 577

- Driver, S. P., et al., 2006, MNRAS, 368, 414
- Eisenstein, D. J., Hogg, D. W., et al, 2003, ApJ, 585, 694E
- Ellison, S. L., et al, 2010, MNRAS, 407, 1514
- Fassano, G .et al, 2000, ApJ, 542, 673
- Faber, S. M. et al., 2007, ApJ, 665, 265
- Fang, J. J., Faber, S. M, Salim, S, et al., 2012, ApJ, 761, 23
- Feruglio, C., Maiolino, R., Piconcelli, E. et al, 2010, A&A, 518, 155
- George, S. et al., 2011, ApJ, 742, 125
- Giodini, M. G. et al.,2012, A&A, 538, 104
- Glasser, G. J., 1962, J. Amer. Stat. Assoc., 57, 648
- Goncalves, T. S. et al., 2012, ApJ, 759, 67
- Haines, C. P. et al., 2006, ApJ, 657L, 21H
- Haines, C. P., et al. 2006, ApJ, 647, L21
- Haines, C. P., Gargiulo A. & Merluzzi, P., 2008, MNRAS, 385, 1201
- Hasinger G., Cappelluti N., et al., 2007, ApJS, 172, 29
- Ideue, Y., Taniguchi, Y. et al., 2012, ApJ, 747, 42
- Ilbert O., Capak P., Salvato M. et al., 2009, ApJ, 690, 1236
- Ilbert, O., Salvato, M. et al., 2010 ApJ, 709, 644
- Kauffmann, G, Heckman, T. M, White, S.D.M, et al., 2003, MNRAS, 341, 33
- Kauffmann G, Heckman T. M, Tremonti C, et al., 2003, MNRAS, 346, 1055
- Kauffmann, G, Cheng, Li, Jian, Fu, et al., 2012, MNRAS, 422, 997
- Kawata, D.& Mulchaey, J. S., 2008, ApJ, 672, L103
- Kenneth C. W., et al., 2011, ApJ, 728, 119
- Koekemoer, A. M., Aussel, H. et al., 2007, ApJS, 172,196

- Kong, X., Fang, G., Arimoto, N., & Wang, M. 2009, *ApJ*, 702, 1458
- Kováč., et al., 2010, *ApJ*, 718, 86
- Lacy, M. et al., 2004, *ApJS*, 154, 166
- Lambas, D. G., Tissera, P. B., Alonso M. S, Coldwell, G., 2003, *MNRAS*, 346, 1189
- Li, C., Kauffmann, G., Heckman, T. M., et al., 2008, *MNRAS*, 385, 1903
- Lilly, S. J., Le Fèvre, Renzini, A., et al., 2007, *ApJS*, 172, 70
- Lotz, J. M., Primack, J. & Madau, P., 2004, *AJ*, 128, 163
- Lotz, J. M., Madau, P. et al., 2006, *ApJ*, 636, 592
- Lubin, L. M., Oke J. B., & Postman, M., 2002, *AJ*, 124, 1905L
- Lusso, E., Comastri, A., Vignali, C., et al. 2011, *A&A*, 534, A110
- Marino, A. Bianchi, L., Rampazzo, R., et al., 2011, *ApJ*, 736, 154
- Martig, M. Bournaud, F., Teyssier, R. & Dekel, A., 2009, *ApJ*, 707, 250
- Martin, D. C. et al., 2007, *ApJS*, 173, 342
- McCarthy, I. G. et al., 2008, *MNRAS*, 38,593
- McNamara B. R. et al., 2000, *ApJ*, 534, L135
- McNamara, B. R. & Nulsen, P. E. J., 2007, *ARA&A*, 45, 117
- Mendez, A. J., et al. 2011, *ApJ*, 736, 110
- Mendez, A. J., et al. 2013, *ApJ*, 770, 40
- Mobasher, B. et al., 2007, *ApJS*, 172, 117
- Moran, S. M. Ellis, R. S. et al., 2007, *ApJ*, 671, 1503
- Moresco, M., Pozzetti, L. et al., 2010, *A&A*, 524, 67
- Moustakas, J., Coil, A. L., Aird, J. et al., 2013, *ApJ*, 767, 50
- Nandra, K., Georgakakis, A. et al., 2007, *ApJ*, 660, L11
- Nikolic, B, Cullen, H & Alexander, P., 2004, *MNRAS*, 355, 874

- Page, M. J., Symeonidis, M, Vieira, J. D., et al., 2012, *Nature*, 485, 213
- Pan, Z. Z., Yuan, Q. R., Kong, X. et al., 2012, *MNRAS*, 421, 36
- Patton., et al., 2011, *MNRAS*, 412, 591
- Peng Y. J., et al., 2010, *ApJ*, 721, 193
- Perez, J. et al., 2009, *MNRAS*, 399, 1157
- Polletta, M. et al., 2007 *ApJ*, 663, 81
- Pozzetti, L. et al., 2010, *A&A*, 523, A13
- Prevot, M, L., et al, *A&A*, 132, 389
- Rampazzo, R., Marino, A., Tantalò, R., et al., 2007, *MNRAS*, 381, 245
- Robertson, B. et al., 2006, *ApJ*, 645, 986
- Rosario, D. J et al., 2013, *ApJ*, 763, 59
- Rosario, D. J et al., 2013, *ApJ* accepted, arXiv:1302.1202v2
- Salim, S. et al., 2005, *ApJ*, 619, L39
- Salim, S., et al., 2007, *ApJS*, 173, 267
- Salim, S. et al., 2009, *ApJ*, 700, 161
- Salim, S. Fang, J. J, Rich, R. M, et al., 2012, *ApJ*, 700, 161
- Sanders, D. B., Salvato, M, Aussel H., et al., 2007, *ApJS*, 172, 86
- Salvato, M. et al., 2009, *ApJ*, 690, 1250
- Scalata, C., Carollo, C. et al. 2007, *ApJS*, 172, 406
- Scoville, N., Aussel, H., Brusa, M., et al., *ApJS*, 172, 1
- Schiavon R. P., 2007, *ApJS*, 171, 146
- Shu, Y. P, et al., *AJ*, 143, 90S
- Silverman, J. D., Lamareille, F., Maier, C., et al. 2009, *ApJ*, 696, 396
- Smith, R. J., et al., 2010, *MNRAS*, 408, 1417

- Snyder, G. F., et al., 2011, *ApJ*, 741, 77s
- Springel, V., Di Matteo T., & Hernquist, L., 2005, *ApJ*, 620, L79
- Stern, D., et al., 2005, *ApJ*, 631, 163
- Strateva, I. V et al., 2001, *AJ*, 122, 1861
- Sturm, E. et al., 2011, *ApJ*, 733, 16
- Tasca, L. A. M, et al., 2009, *A&A*, 503, 379
- Thomas, D., Maraston, C., Bender, R., Mendes de Oliveira C., 2005, *ApJ*, 621, 673
- Thomas, D., Maraston, C., Schawinski, K., et al., 2010, *MNRAS*, 404, 1775
- Tremonti, C. A, Moustakas, J, Diamond, S., & Aleksandar, M., 2007, *ApJ*, 663, 77
- Thilker, D., et al., 2010, *ApJ*, 714, L171
- van den Bosch, F. C., Aquino, D., Yang, X. H. et al., 2008, *MNRAS*, 387, 79
- van der Wel, A., et al., 2010, *ApJ*, 714, 1779
- Vogt, N. P, Haynes, M. P, Giovanelli, R. & Herter, T., 2004, *AJ*, 127, 3300
- Wang, T. et al., 2012, *ApJ*, 752, 134
- Weinmann, S. M., et al., 2010, *MNRAS*, 406, 2249
- Whitaker, K. E., et al., 2010., *ApJ*, 719, 1715
- Willmer C. N. A, Faber, S. M. et al., 2006, *ApJ*, 647, 853
- Williams R, J., et al., 2009, *ApJ*, 691, 1879
- Williams R, J., et al., 2007, *ApJS*, 173, 293
- Xue, Y. Q., Brandt, W. N. et al., 2010, *ApJ*, 720, 368
- Yan, R. et al., 2011, *ApJ*, 728, 38
- Zamojski, M. A., Schiminovich, D. et al., 2007, *ApJS*, 172, 468 6
- Zehavi I., Zheng Z. et al., 2011, *ApJ*, 736, 59
- Zhu, G. T., Blanton, M. R. & Moustakas J., 2010, *ApJ*, 722, 491

Table 1: Low mass limit and galaxy number of blue, green and red sample in each redshift bin

redshift	mass limit $\log(M/M_{\odot})$	N_{blue}	N_{green}	N_{red}
0.2-0.3	8.4	3101	156	842
0.3-0.4	8.7	5522	405	1824
0.4-0.5	8.9	3763	303	1072
0.5-0.6	9.1	3327	286	794
0.6-0.7	9.4	3751	453	1599
0.7-0.8	9.5	3198	189	1157
0.8-0.9	10.0	2068	345	1927
0.9-1.0	10.3	1265	210	1278

Table 2: B_{ZEST} for disk galaxies.

redshift	mass range $\log(M/M_{\odot})$	galaxy number	B_{blue}^a	B_{green}	B_{red}
0.2-0.3	10.0-11	26	[4,11, 9, 2]	[3,11, 9, 3]	[16,19, 1, 0]
0.3-0.4	10.0-11	94	[12,38,32,12]	[27,41,25, 1]	[50,40, 4, 0]
0.4-0.5	10.0-11	99	[12,37,37,13]	[23,52,22, 2]	[46,50, 3, 0]
0.5-0.6	10.0-11	108	[10,38,37,23]	[26,56,20, 6]	[43,55, 9, 1]
0.6-0.7	10.0-11	191	[17,63,64,47]	[41,88,47,15]	[57,114,17,3]
0.7-0.8	10.0-11	85	[9,25,27,23]	[11,46,21, 7]	[26,49, 9, 1]
0.8-0.9	10.0-11	170	[22,52,55,41]	[29,80,39,22]	[49,98,22, 1]
0.9-1.0	10.0-11	90	[10,29,30,21]	[14,43,26, 7]	[22,61, 6, 1]
0.2-0.3	<10.0	65	[2,15,34,14]	[2,27,33, 3]	[5,30,36, 4]
0.3-0.4	<10.0	123	[3,28,62,30]	[9,46,58,10]	[8,72,41, 2]
0.4-0.5	<10.0	59	[2,15,25,17]	[1,28,25, 5]	[6,31,21, 1]
0.5-0.6	<10.0	31	[1, 6,13,11]	[1,13,14, 3]	[5,16,10, 2]
0.6-0.7	<10.0	50	[1,10,17,22]	[1,20,23, 6]	[2,28,17, 3]

^aNumber of disk galaxies classified as $B_{\text{ZEST}} = [0, 1, 2, 3]$. For red and blue galaxies, the number is averaged over 15 different comparison samples, respectively.

Table 3: Results of KS statistical tests applied to the Σ_{10} distribution in green galaxies and comparison sample.

redshift	mass range $\log(M/M_{\odot})$	galaxy number	Probability $KS_{\text{green-red}}$	Probability $KS_{\text{green-blue}}$
0.2-0.3	<10.0	99	0.1634	5.35E-5
0.3-0.4	<10.0	201	0.1913	2.6E-14
0.4-0.5	<10.0	106	0.4676	0.00013
0.5-0.6	<10.0	66	0.0389	0.01625
0.6-0.7	<10.0	74	0.1497	0.08104
0.2-0.3	10.0-11	33	0.2636	0.86874
0.3-0.4	10.0-11	138	0.6733	0.00331
0.4-0.5	10.0-11	137	0.0959	0.65454
0.5-0.6	10.0-11	150	0.0514	0.12042
0.6-0.7	10.0-11	261	0.6705	8.27E-5

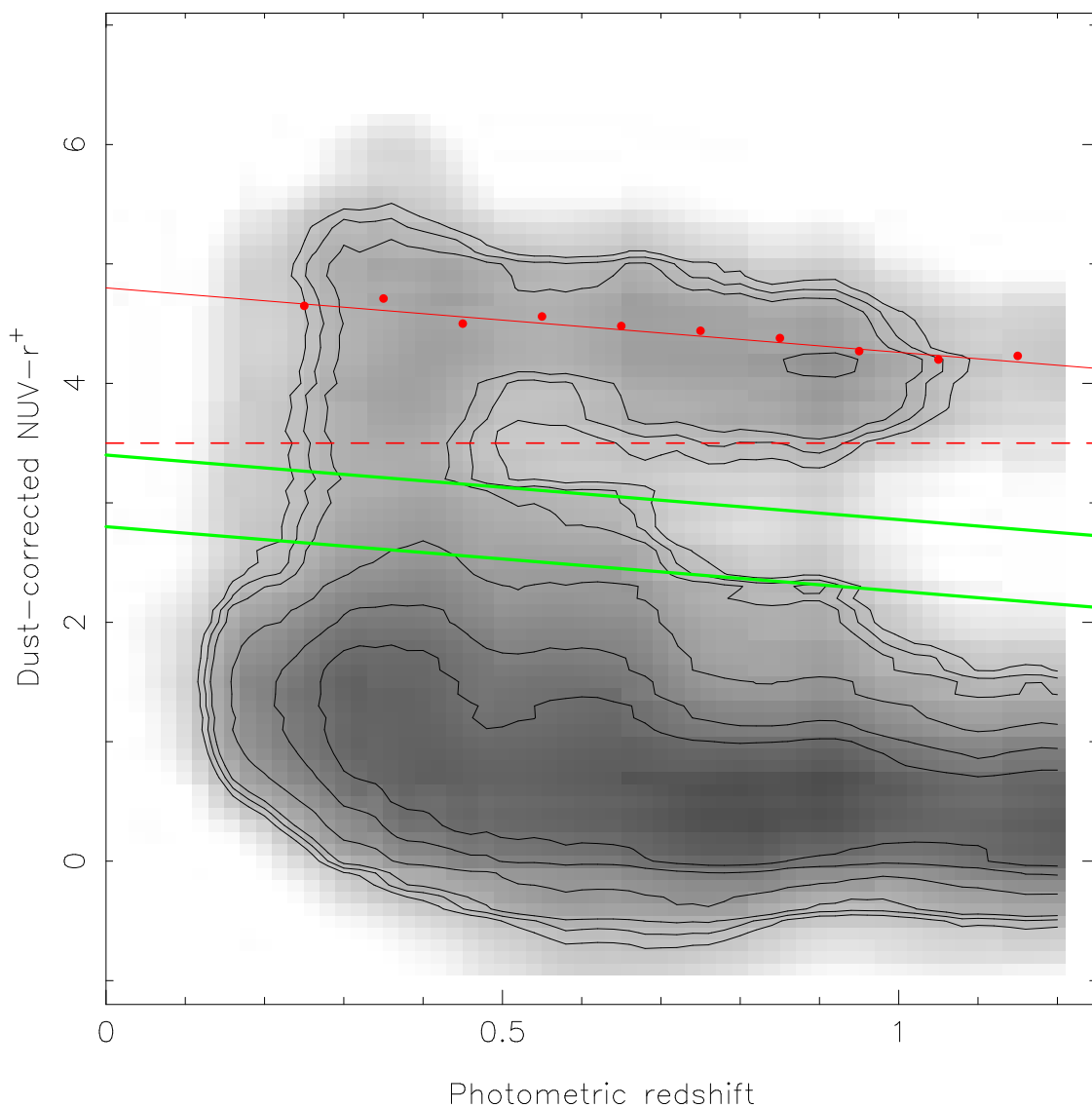


Fig. 1.— Rest-frame $(\text{NUV}-r^+)_{\text{corr}}$ color as a function of redshift for galaxies with $i^+ < 24.0$ and $M_* > 10^{8.0} M_\odot$ at $z < 1.2$. The grayscale represents the galaxy number density. The contours are plotted to clarify the bimodal color distribution. The red solid line is the linear fit of the medium color of “quiescent galaxies”. Red dashed line presents the color cut utilized to separate “quiescent” galaxies, as quoted in Ilbert et al. (2010). The red solid circles mark the medium color for “quiescent” galaxies within the redshift range of $0.2 < z < 1.2$. The two green solid lines show the selection criteria of green galaxies.

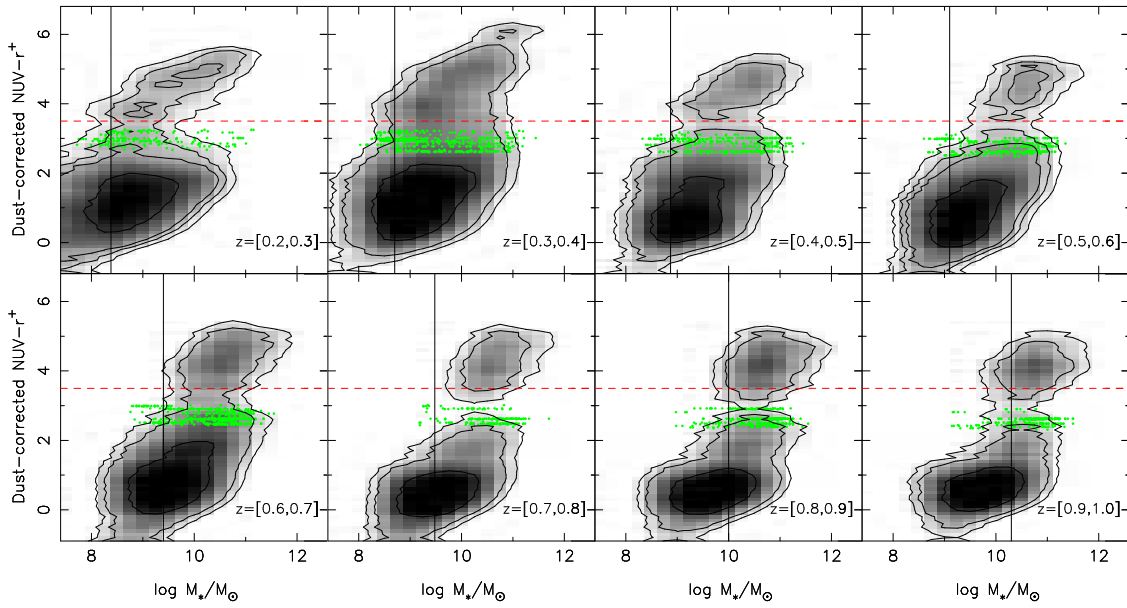


Fig. 2.— $(\text{NUV} - r^+)_{\text{corr}}$ color as a function of stellar mass for galaxies with $i^+ < 24.0$ within the redshift range of $z = [0.2, 1.0]$. The grayscale represents galaxy number density. Red dashed line denotes the color cut of $(\text{NUV} - r^+)_{\text{corr}} = 3.5$. Green dots are green galaxies that meet our selection criterion. Solid vertical line shows our low mass limit for each redshift bin.

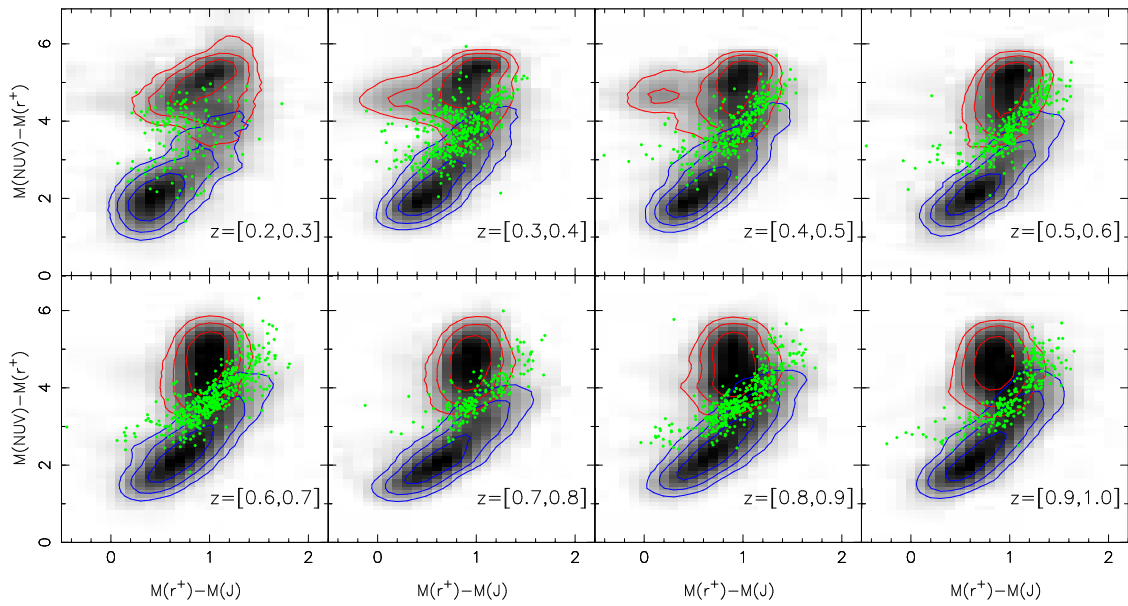


Fig. 3.— Rest-frame $M(\text{NUV}) - M(r^+)$ vs. $M(r^+) - M(J)$ (no dust-corrected) from $z = 0.2$ to $z = 1.0$, for galaxies above low mass limit. The grayscale represents galaxy number density. Red and blue contours include 95%, 80% and 60% of red and blue galaxies, respectively. Green dots denote green galaxies in our sample.

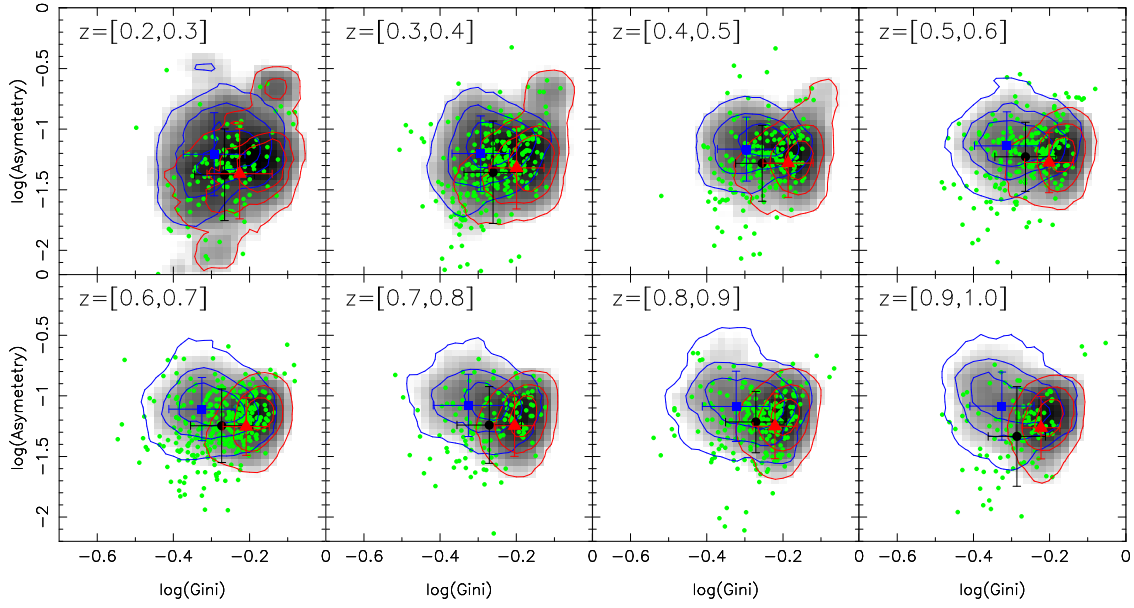


Fig. 4.— The Gini coefficient (G) vs. asymmetry (A) diagram. Green galaxies are denoted as green dots. The numbers of the red and blue compared sample are 15 times as that of the green sample. The grayscale represents galaxy number density of comparison sample. The red and blue contours enclose 30%, 60% and 90% of the red and blue galaxies, respectively. Blue square, black circle and red triangle mark the average Gini coefficient and asymmetry of the blue, green and red sample, respectively. The error bars are the standard deviations of G and A distributions for each sample.

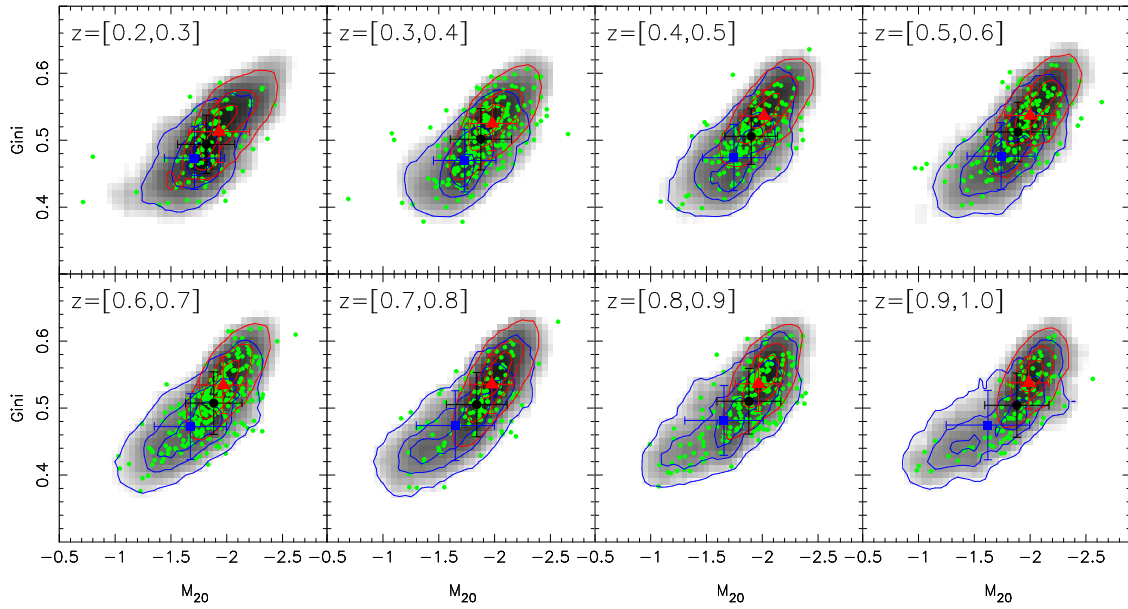


Fig. 5.— The M_{20} vs. Gini diagram. Symbols are the same as in Figure 4.

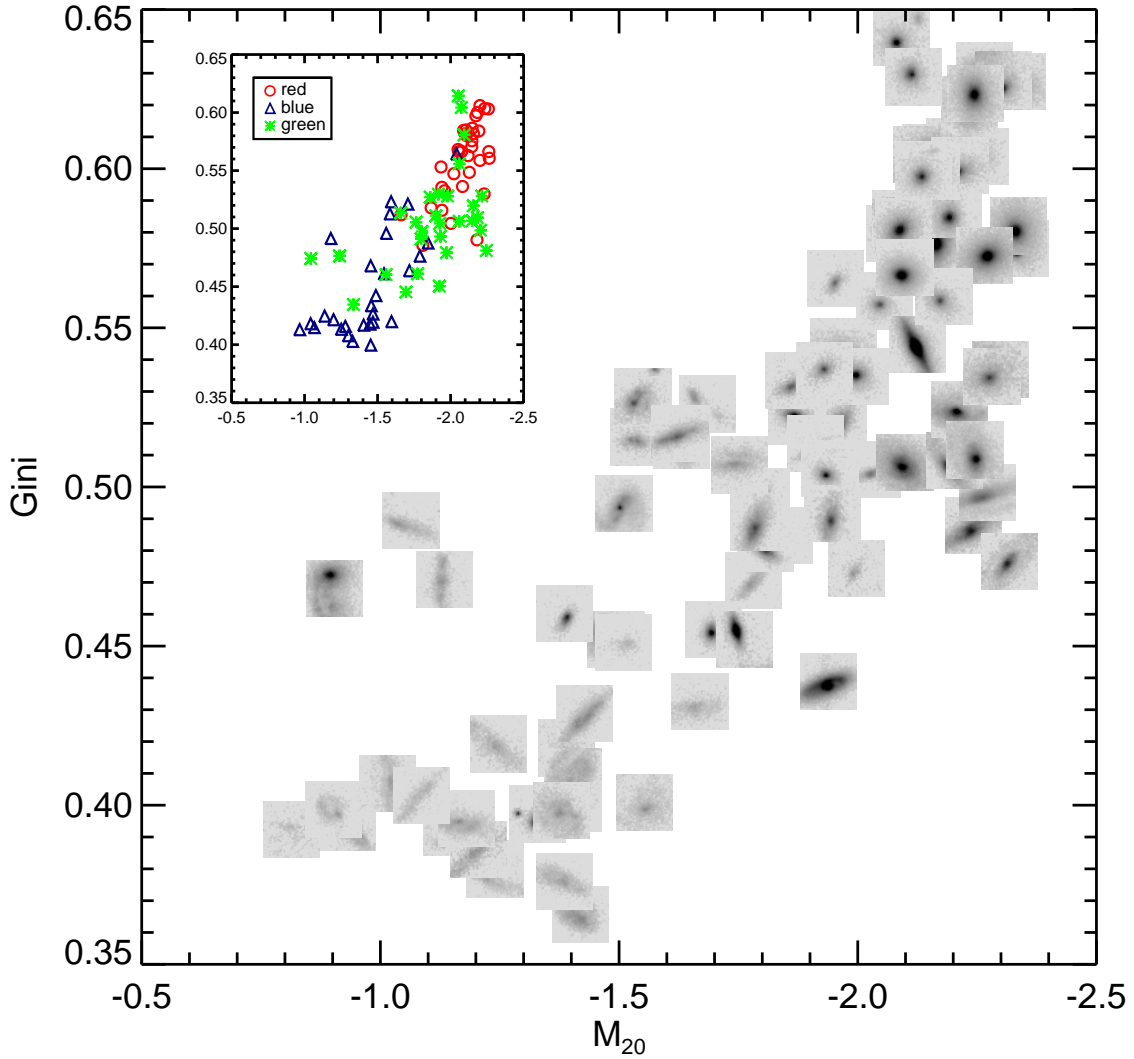


Fig. 6.— The M_{20} vs. G diagram for some randomly selected galaxies at $0.6 < z < 0.7$. Red, green, blue galaxies are denoted with red circles, green crosses and blue triangles, respectively. The HST/ACS postage-stamp images for each subsample represent morphologies for galaxies in various locations of this diagram.

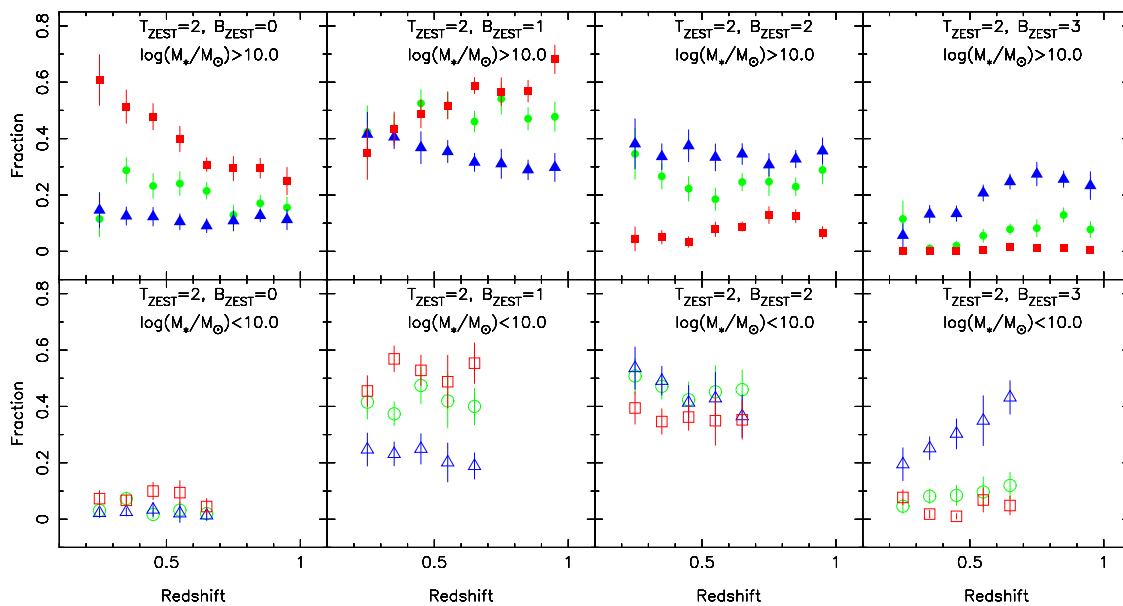


Fig. 7.— The fraction of red, blue and green disk galaxies with different B_{ZEST} parameter as a function of redshift. For a certain subsample, the fraction is defined as the disk galaxy number with a certain B_{ZEST} in the subsample divided by the total disk galaxy number in the subsample in that redshift bin. Blue galaxies are indicated in blue triangles, green galaxies in circles, and red galaxies in squares. For blue and red compare samples, the error bars are the 1σ standard deviations of 15 resamplings. The error bars of green galaxies are derived from 1000 bootstrap resamplings.

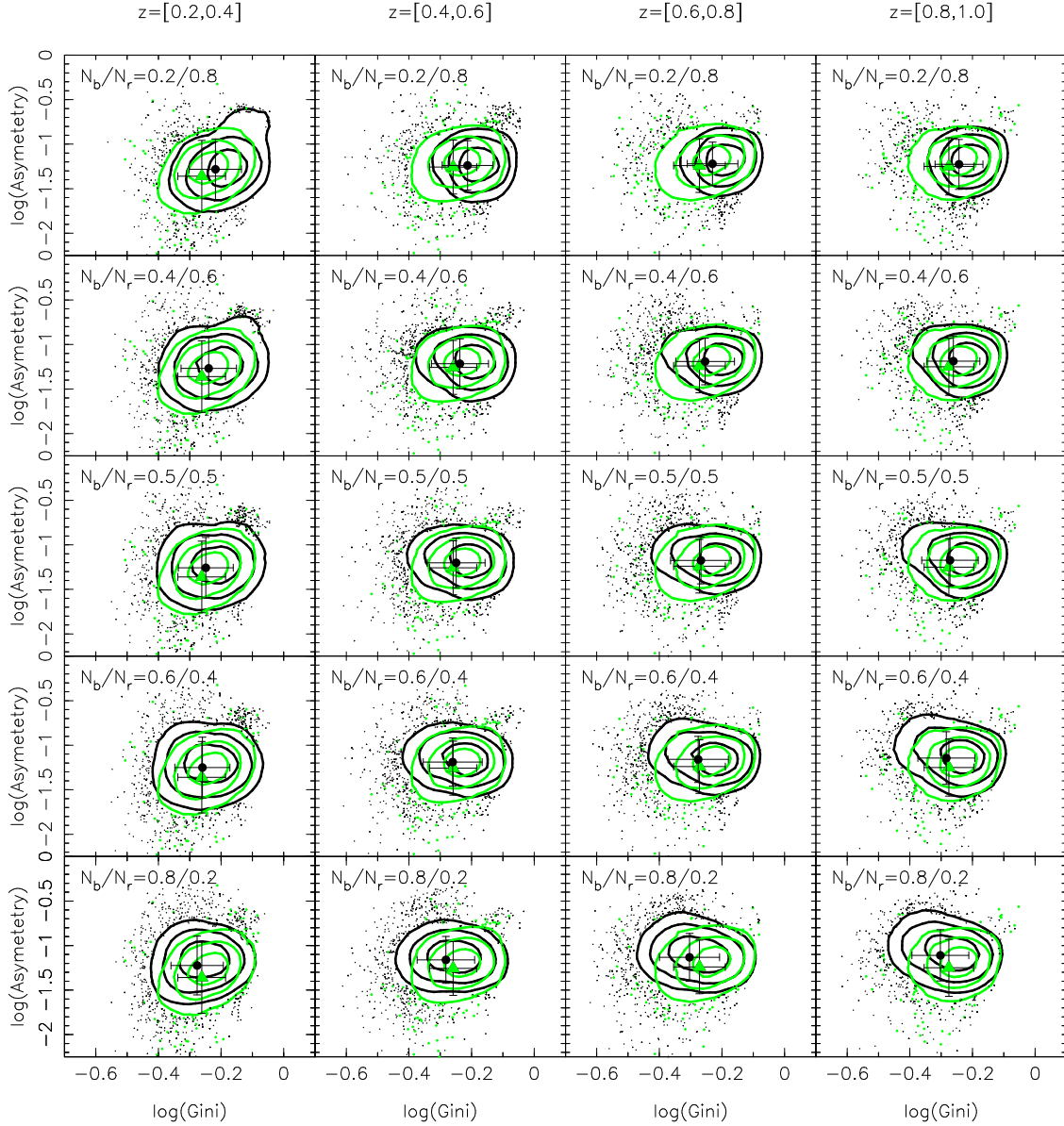


Fig. 8.— The Gini coefficient (G) vs. asymmetry (A) diagram for green galaxies and mixed sample. Green galaxies are denoted as green dots. The green and black contours enclose 30%, 60% and 80% of the green and mixed galaxies, respectively. Green triangle and black circle mark the average $Gini$ coefficient and $Asymmetry$ of green and mixed sample, respectively. The error bars are the standard deviations of $Gini$ and $Asymmetry$ distribution for each sample. The blue to red ratio N_b/N_r is marked in the top left in each panel.

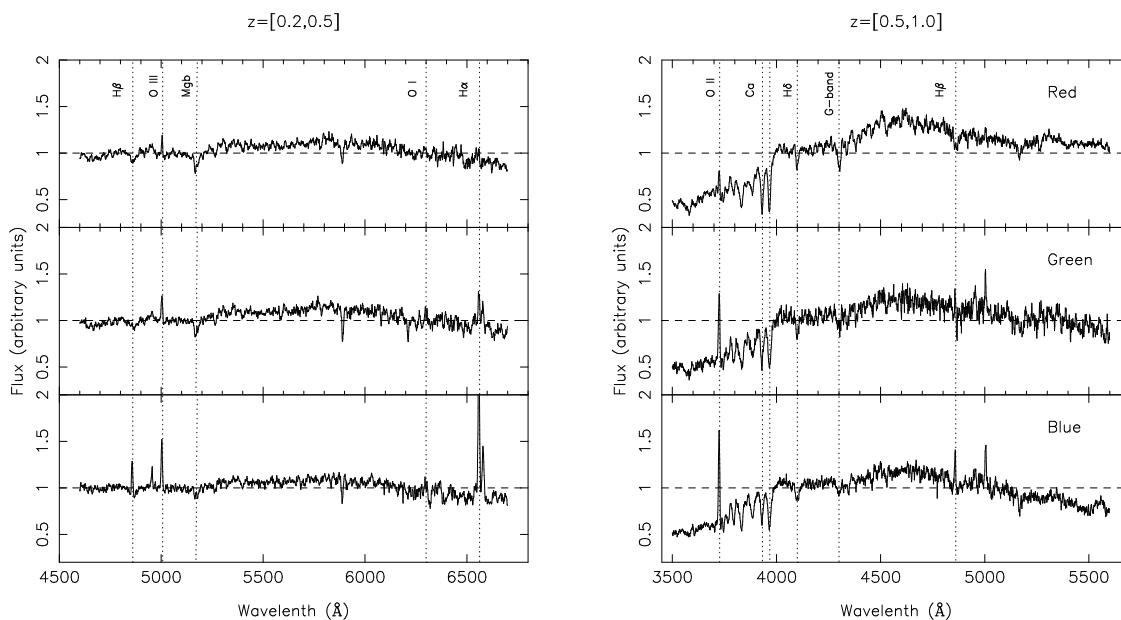


Fig. 9.— The stacked spectra of blue, green and red galaxies. The left panels show the stacked spectra at the low redshift bin $z=[0.2, 0.5]$. The blue, green and red spectrum are stacked by 378, 86, 390 spectra, respectively. The spectra are normalized to the average flux between 5050 \AA and 5100 \AA . The vertical dotted lines show the ordinary emission lines or absorption lines. The right panels show the stacked spectra at the high redshift bin $z=[0.5, 1.0]$. The red, green and blue spectrum are stacked by 456, 118 and 348 spectra, respectively, and normalized to the average flux between 4050 \AA and 4100 \AA .

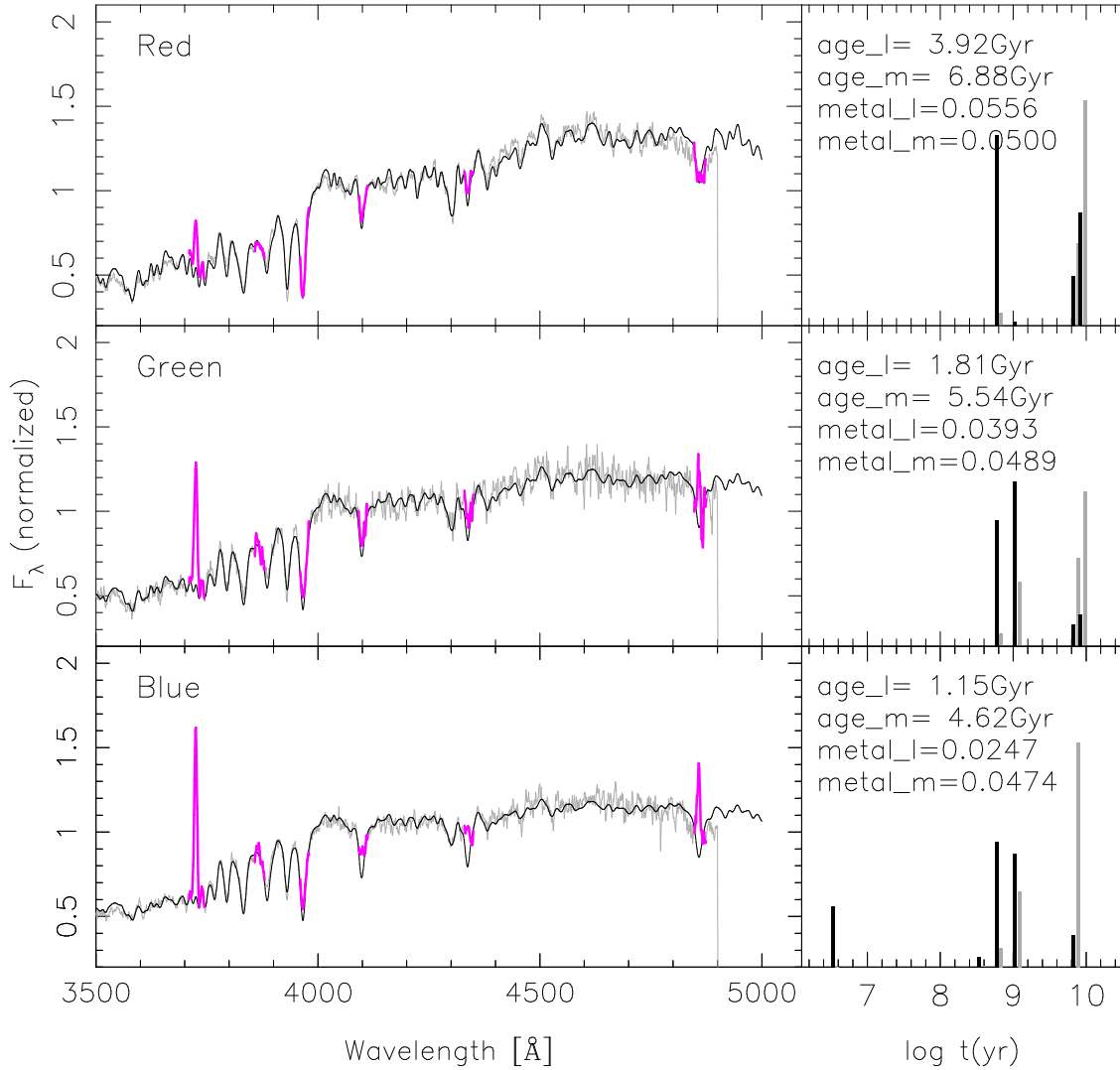


Fig. 10.— The results of STARLIGHT fitting on the stacked spectra. In the left panels, the stacked spectra are shown in grey lines, and the best fitting spectra are shown in black solid lines. The pink lines show the masked regions. In the right panels, the solid black histograms show the flux-weighted SSP vectors, while the grey histograms show the mass-weighted vectors. The flux-weighted age, mass-weighted age, flux-weighted metallicity and mass-weighted metallicity are shown from top to bottom.

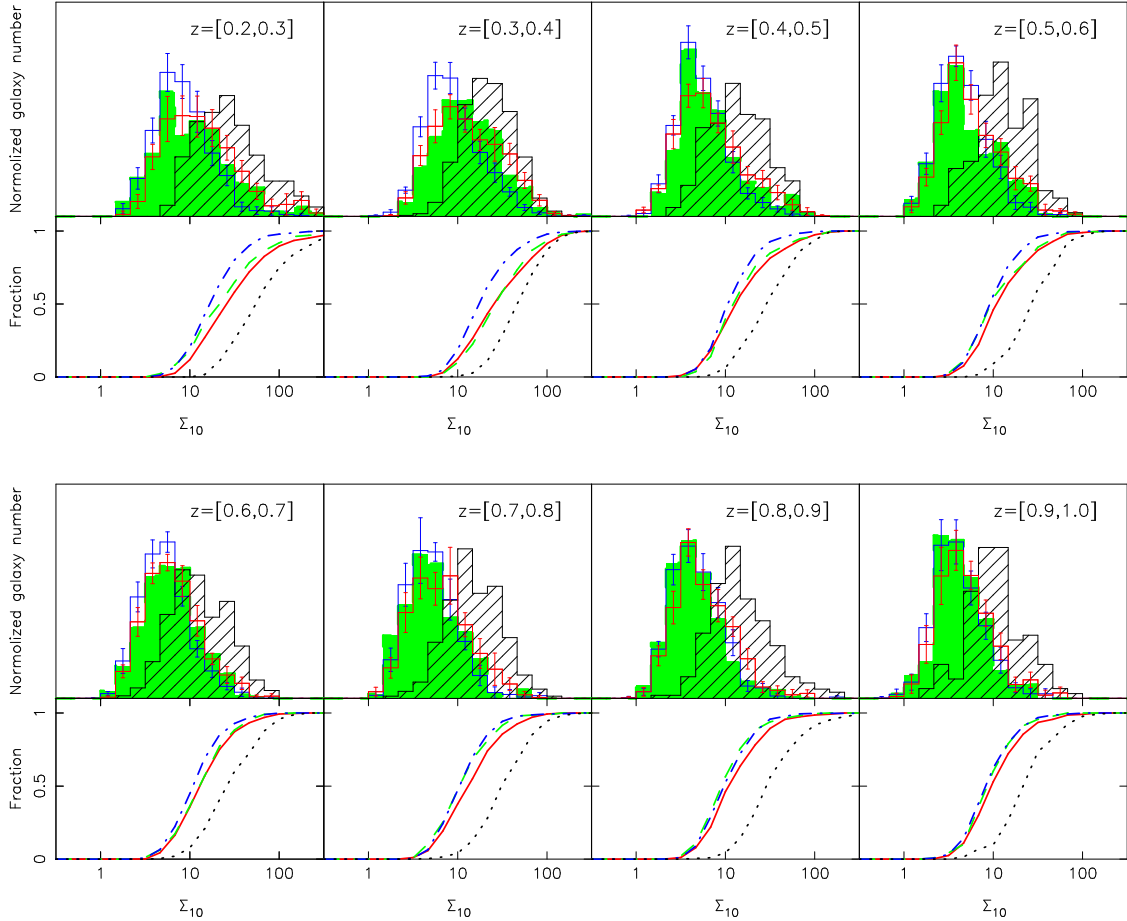


Fig. 11.— Σ_{10} distributions of blue (blue solid), green (green filled), red galaxies (red solid) and X-ray group members (black shaded). The histogram of blue, red and group members have been normalized to have same effective area with that of green galaxies. The blue and red histograms are averaged over the Σ_{10} distribution of 15 different comparison samples, and errorbars are the standard deviations of galaxy number in that Σ_{10} bin. The smaller panels below each histogram show the cumulative fraction distributions (blue galaxies: dot-dashed lines; green galaxies: dashed lines; red galaxies: solid lines; X-ray group members: dotted lines.).

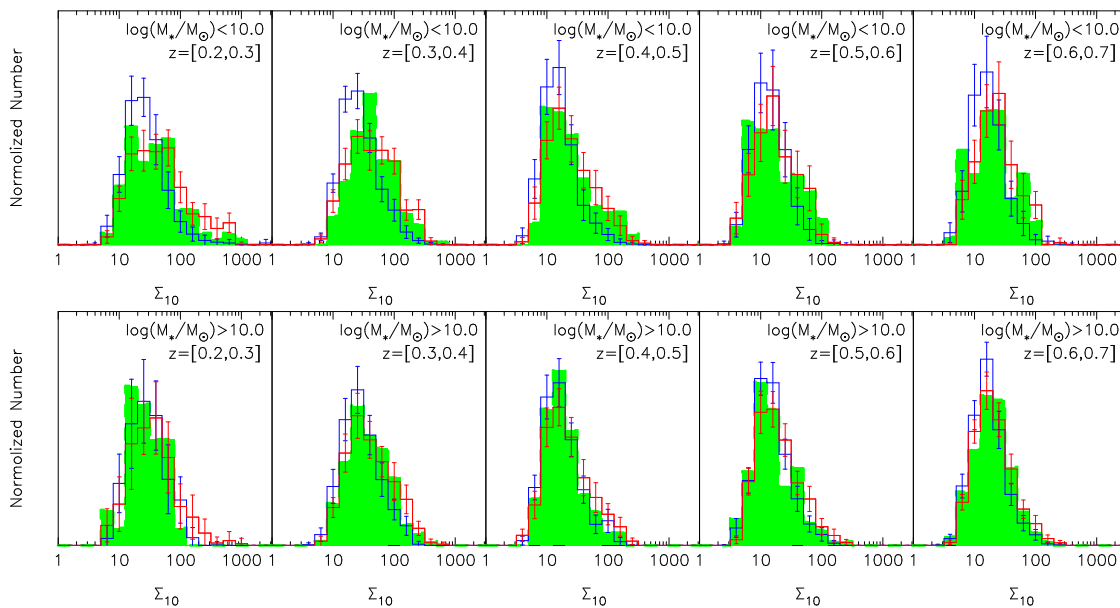


Fig. 12.— Σ_{10} distributions of blue (blue dashed), green (green filled), red galaxies (red solid) at $z = [0.2, 0.7]$, shown into 2 mass bin: $\log(M_*/M_\odot)=[10.0,11.0]$ and $\log(M_*/M_\odot)<10.0$.

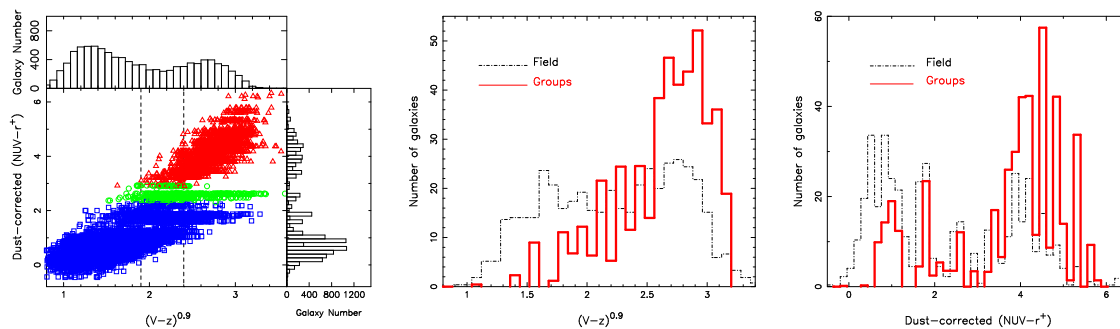


Fig. 13.— Left panel: the color-color diagram (k-corrected $(V-z)^{0.9}$ vs. $(NUV-r^+)_{\text{corr}}$) at $0.8 < z < 1.0$, along with the histograms of k-corrected $(V-z)^{0.9}$ color and $(NUV-r^+)_{\text{corr}}$. Blue, green and red galaxies are marked as blue squares, green circles and red triangles, respectively. The dashed vertical lines indicate the green valley definition of Balogh et al. (2011). It is clear that the two criteria are different and only about 30% green galaxies selected with Balogh et al. (2011) criterion meet our selection criterion. middle panel: The k-corrected $(V-z)^{0.9}$ color histograms for group members ($P_{\text{mem}} \geq 0.1$, red solid line) and field galaxies ($P_{\text{mem}} = 0.0$ and $\log(\Sigma_{10}) < 0.5$, black dot-dashed line) with $M_* > 10^{10.1} M_\odot$. The field galaxy histogram has been normalized and has the same area as the group galaxy histogram. Right panel: $NUV-r^+$ color distribution for field and group galaxies with $M_* > 10^{10.1} M_\odot$.